Contrib Mineral Petrol (2016) 171:50
DOI 10.1007/s00410-016-1255-7

ORIGINAL PAPER

An experimental investigation of the stability of majoritic garnet in the Earth's mantle and an improved majorite geobarometer

C. H. Wijbrans[1,2] · A. Rohrbach[1] · S. Klemme[1]

Received: 11 June 2015 / Accepted: 28 March 2016 / Published online: 3 May 2016

Abstract The stability of the majorite component in garnet has been experimentally investigated at high pressure and high temperature, focusing on the effect of bulk composition and temperature. High-pressure experiments were performed in a multi-anvil apparatus, at pressures ranging from 6 to 14.5 GPa, and temperatures between 1400 and 1700 °C. Experiments were performed in a range of bulk compositions in the system SiO_2–Al_2O_3–Cr_2O_3–CaO–MgO with varying Cr/(Cr + Al) ratios. The majorite content of garnet gradually increases with pressure, and the composition of the garnet, specifically the Cr/(Cr + Al) ratio, exerts a significant effect on the majorite substitution. We found no significant effect of temperature. We use the experimental results in combination with the literature data to derive two empirical geobarometers, which can be used to determine the equilibration pressure of natural majoritic garnets of peridotitic and eclogitic bulk compositions. The barometer for peridotitic compositions is

$$P = -77.1 + 27.6 \times Si + 1.67 \times Cr$$

And the barometer for eclogitic compositions is

$$P = -29.6 + 11.8 \times Si + 7.81 \times Na + 4.49 \times Ca.$$

Communicated by Mark S Ghiorso.

Electronic supplementary material The online version of this article (doi:10.1007/s00410-016-1255-7) contains supplementary material, which is available to authorized users.

✉ C. H. Wijbrans
clazina.wijbrans@erdw.ethz.ch

[1] Institut für Mineralogie, Westfälische Wilhelms Universität Münster, Corrensstrasse 24, 48149 Münster, Germany

[2] Present Address: Institute of Geochemistry and Petrology, ETH Zürich, Clausiusstrasse 25, 8092 Zurich, Switzerland

Keywords Majorite · Garnet · Chromium · Diamond inclusions · Depleted mantle · Transition zone · Multi-anvil apparatus · Geobarometry · Deep Earth mantle

Introduction

Garnet is stable in a wide range of geological settings, and it commonly occurs in igneous and metamorphic rocks, occasionally also in sedimentary rocks, and is one of the main mineral phases in the Earth's upper mantle (Wood et al. 2013). Garnet is the most important host for Al in the deeper upper mantle (e.g., O'Neill 1981; Klemme and O'Neill 2000a) and a major sink for many trace elements. It is stable up to very high pressures, well into the transition zone, until it breaks down to $CaSiO_3$ perovskite, bridgmanite ($MgSiO_3$ perovskite), and an aluminous phase between 25 and 30 GPa (e.g., Ono et al. 2001).

Pyroxene, another important mineral that is stable in the upper mantle, also undergoes a series of high-pressure phase transformations: Enstatite ($MgSiO_3$ pyroxene) or its high-pressure polymorphs will eventually adopt the garnet structure at approximately 20 GPa (Kato 1986). This isochemical garnet end member ($MgSiO_3$) is called majorite (Ringwood and Major 1966). In more complex compositions, the pyroxene-to-majorite phase transformation does not occur as a sharp phase boundary. Instead, at pressures of around 5 GPa, pyroxene begins to form a solid solution with garnet (Ringwood and Major 1966, 1971; Akaogi and Akimoto 1977). As a result, the molar proportion of garnet in the mantle increases rather dramatically with increasing pressure while the molar pyroxene proportion decreases (e.g., Frost 2008). The garnet–pyroxene solid solution reaction continues into the transition zone, up to pressures of approximately 14.5 GPa, until all pyroxene is exhausted (Irifune 1987).

Majoritic garnet

A normal garnet can be described by the general mineral formula $X_3Y_2Si_3O_{12}$, where the dodecahedral X-site is usually occupied by the divalent elements Ca, Mg, and Fe^{2+}, and the octahedral Y-site by the trivalent elements Al, Cr, and Fe^{3+}. In normal garnets, Si^{4+} resides in the tetrahedral site only. However, with increasing pressure, Si partitions increasingly into the octahedral (Y-site) as well. This implies that the Si content of garnet will increase at the expense of the other elements on the Y-site, which is usually mainly Al. The resulting garnet–pyroxene solid solution is referred to as majoritic garnet or simply as "majorite." By definition, a garnet has a majorite component when it contains octahedrally coordinated Si, i.e., the Si cation content is larger than 3.00 for a total of 12 oxygen. When taking into account the uncertainties of electron microprobe measurements, the cutoff point of 3.05 Si is often used.

The majorite transformation reaction between pyrope ($Mg_3Al_2Si_3O_{12}$) and enstatite ($MgSiO_3$) may be described as

$$(1-x)\,Mg_3Al_2Si_3O_{12} + 4x\,MgSiO_3 = Mg_3\left(Mg_xSi_xAl_{(2-2x)}\right)Si_3O_{12} \quad (1)$$

where one Mg^{2+} is substituted together with one Si^{4+} for two Al^{3+} to achieve charge balance. When Na-rich pyroxenes are present, a different substitution mechanism can also take place: Because Na is monovalent, the coupled substitution of a divalent element together with Si^{4+} is not required. The incorporation of octahedral Si can instead be achieved with the substitution mechanism: $M^{2+} + Al^{3+} = Na^{+} + Si^{4+}$ (where M is a divalent element, e.g., Mg or Fe^{2+}) (Bindi et al. 2011).

Natural majoritic garnets

As majoritic garnet is a high-pressure mineral phase, it is only rarely found in natural rock samples. In orogenic peridotites (for instance in the Western Gneiss region of Norway), samples are found which contain garnets with pyroxene exsolutions that are commonly interpreted to represent former majoritic garnets (Van Roermund et al. 2000, 2001; Scambelluri et al. 2008). Similar pyroxene exsolutions are also found in garnets from mantle xenoliths derived from kimberlites (Haggerty and Sautter 1990; Roden et al. 2006; Alifirova et al. 2012). Most importantly, perhaps, majoritic garnets are sometimes observed as inclusions in diamonds (Haggerty and Sautter 1990). While rare, majoritic diamond inclusions are reported from cratons all over the world (e.g., Haggerty and Sautter 1990; Sautter et al. 1991; Stachel 2001; Banas et al. 2007; Collerson et al. 2010; Harte 2010; Kiseeva et al. 2013b).

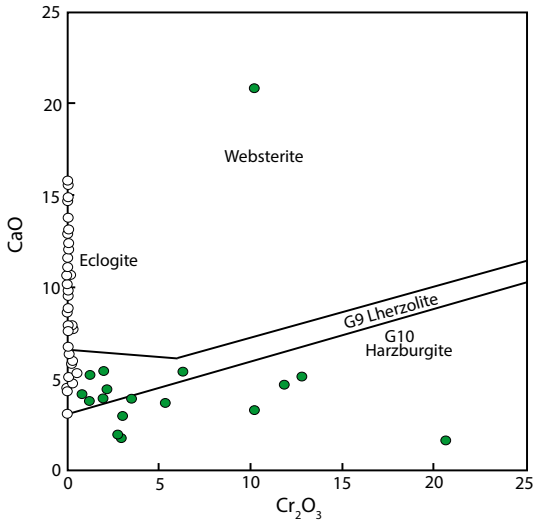

Fig. 1 Garnet classification diagram after (Sobolev et al. 1973, Grutter et al. 2004). The CaO content in garnet is plotted against Cr_2O_3. This diagram can be used to determine the lithology of the source rock that the garnets are derived from. CaO-rich, Cr_2O_3-poor garnets are classified as eclogitic garnets, and CaO-poor, Cr_2O_3-containing garnets are classified as peridotitic, with a further subdivision between lherzolithic (higher CaO) and harzburgitic (lower CaO). Garnets high in both Cr and Ca are websteritic. A number of majoritic garnets from diamond inclusions are also plotted in the diagram (for references, see Table 5). The eclogitic garnets included in diamonds are plotted as *white circles,* and the peridotitic (Cr containing) garnets are depicted as *green circles*. Although it is not very clear due to the samples of eclogitic compositions overlapping a lot, the majoritic garnets of eclogitic compositions are much more abundant than majoritic garnets from peridotitic compositions

The composition of non-majoritic garnet inclusions in diamonds is often used to determine the lithology of the source rock (Schulze 2003; Grutter et al. 2004; Stachel and Harris 2008; Cookenboo and Grutter 2010). Mantle-derived garnets are grouped by their lithology using a CaO versus Cr_2O_3 diagram (Fig. 1) (Sobolev et al. 1973; Grutter et al. 2004). In this diagram, high-CaO and low-Cr_2O_3 garnets are categorized as eclogitic garnets, high-Cr_2O_3 and high-CaO garnets as websteritic garnets, and high-Cr_2O_3 and low-CaO garnets are categorized as peridotitic garnets. A further distinction is made within the peridotitic garnets between lherzolitic garnets (higher CaO) which are in chemical equilibrium with clinopyroxene (i.e., Ca-rich pyroxene) and harzburgitic garnets (low CaO). The CaO versus Cr_2O_3 classification diagram can also be used to determine the lithology of majoritic garnets. The compositions of a number of known majoritic garnets that are found worldwide are plotted in Fig. 1. It is important to note that most of the majoritic garnets that are found worldwide have eclogite compositions, while only very few are found with peridotitic compositions (Stachel 2001).

The common interpretation for the origin of the deep eclogitic diamond inclusions is that they are derived from subducted oceanic crust (e.g., Jacob 2004). At high pressures, basaltic rocks from the subducting slabs will transform to eclogite, which may penetrate the Earth's mantle to very large depths (e.g., Widiyantoro and van der Hilst 1996; van der Hilst et al. 1997). The subducting slabs introduce carbon into the mantle, which can lead to the formation of diamond (e.g., Rohrbach and Schmidt 2011; Walter et al. 2011). The relative abundance of eclogitic majorites compared to peridotitic majorites implies either that (1) diamonds are more likely to form in eclogitic rocks at these depths, (2) diamonds that formed in eclogitic source rocks are more likely to be transported to the surface by kimberlite eruptions, or (3) that the garnet content is higher in eclogitic mantle lithologies compared to peridotitic lithologies.

Previous experiments on majorite stability

The occurrence of a solid solution between garnet and pyroxene at high pressures was first suggested by Ringwood and Major (1966) and Ringwood (1967). Since then, several authors have experimentally investigated the solid solution reaction between garnet and pyroxene, and the stability of the majorite component in garnet (e.g., Akaogi and Akimoto 1977, 1979; Irifune 1987; Rohrbach et al. 2007, 2011). The experiments were performed in either simple systems, or in complex, multicomponent (lherzolitic and pyrolitic) compositions. Experiments in eclogitic compositions were published by Gasparik (1989), Ono and Yasuda (1996), Gasparik (2002), Bobrov et al. (2008), Kiseeva et al. (2013a) and Thomson et al. (2016). A number of studies investigated the majorite substitution in a Na-containing system (Gasparik 2002; Bindi et al. 2011; Dymshits et al. 2013). Draper et al. (2003a, b) performed experiments in a Martian mantle composition (i.e., a high Fe bulk composition).

All studies report a significant increase in the majorite component with increasing pressure. Akaogi and Akimoto (1979) investigated the effect of major element composition on majorite stability, comparing phase relations in the $MgO–SiO_2–Al_2O_3$ system to the $FeO–SiO_2–Al_2O_3$ and the $CaO–MgO–SiO_2–Al_2O_3$ systems. They report a large compositional effect: The garnet–pyroxene solid solution occurs at lower pressures in the Fe-containing system and at higher pressures in the Mg–Ca system. The effect of temperature was studied by Akaogi et al. (1987), who conducted experiments at temperatures ranging from 1000 to 1600 °C. They report that the effect of temperature is only minor.

Since then, no systematic study investigated the influence of bulk composition or temperature on majorite stability in the mantle. Furthermore, to our knowledge, there are no experimental studies which investigated the stability of majorite garnets in depleted mantle compositions. This could be important, however, as large parts of the mantle have been subjected to repeated periods of melt extraction (Boyd et al. 1985; Boyd 1989; Walter 2003). Cr is a minor element in the Earth's mantle, but since Cr is more compatible than Al during partial melting, it will become relatively enriched in depleted mantle rocks. Non-majoritic Cr-rich garnets are commonly found as inclusions in diamond derived from the subcontinental lithospheric mantle (Gurney and Switzer 1973, Grutter et al. 2004; Cookenboo and Grutter 2010), implying that these high-Cr garnets are relatively common in the (depleted) mantle. One of the most prominent Cr–garnet end members is knorringite ($Mg_3Cr_2Si_3O_{12}$) which is stable only at pressures above approximately 6 GPa (Ringwood 1977; Irifune et al. 1982; Klemme 2004; Wijbrans et al. 2014; Dymshits et al. 2014; Zou and Irifune 2012; Sirotkina et al. 2015).

Majoritic garnet as a geobarometer

As the majorite substitution in garnet depends mainly on pressure, it has been used to estimate the depth of origin of majoritic garnets. Several authors (e.g., Stachel 2001; Banas et al. 2007; Scambelluri et al. 2008) used the data from Irifune (1987) to estimate pressure of formation of majoritic diamond inclusions. They employed a simple diagram which plots the majorite content (Si cation content) of garnet against the Cr + Al content (Fig. 2). The pressures of the experimental data from Irifune (1987) are added to the diagram and are used to derive a pressure estimate for a garnet from its majorite content. Similarly, Collerson et al. (2000, 2010) used experimental data of several authors to derive an empirical equation to calculate the equilibrium pressures of majorite garnets. When comparing the two methods, the equations of Collerson et al. (2000, 2010) always yield lower pressure for a given majorite content when compared to the Irifune (1987) data. This could be due to the fact that while these equations are based on data from a number of experimental studies (which includes Irifune 1987), the majority of the experiments were done in basaltic or eclogitic bulk compositions while Irifune (1987) used a pyrolitic composition. This obvious discrepancy suggests that there may be a significant effect of bulk composition on majorite forming reaction, and this inspired us to investigate this further. To our knowledge, the effect on Cr on the stability of the majorite component has not been previously investigated in upper mantle phase assemblages, i.e., with garnet in equilibrium with pyroxene. Here, we set out to investigate the effect of bulk composition and temperature on the stability of majorite garnet in depleted mantle compositions.

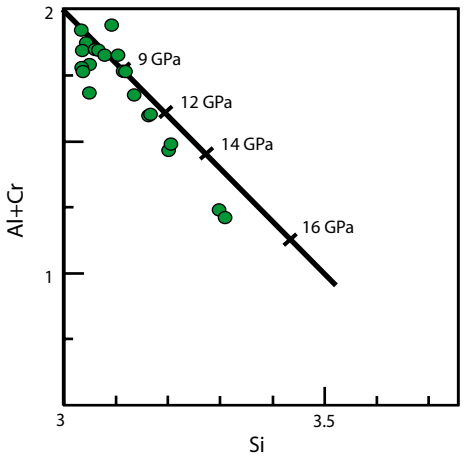

Fig. 2 This diagram is used to estimate the pressures of garnets based on their majorite content. The majorite content (Si cation content) is plotted against Al + Cr. The figure is based on the diagram of Stachel (2001). All data for majoritic garnets should plot on a line with a negative slope, because when the octahedral Si in garnets increases, the Al + Cr content decreases. The pressures for specific majorite contents are indicated in the diagram, derived from experimental data, in this case the data from Irifune (1987). The effect of the composition of the garnet on the majorite content is not taken into account. A number of majoritic garnets of peridotitic compositions (see Fig. 1) are also plotted in the diagram. The data from eclogitic garnets are omitted for clarity, because they mostly overlap with the peridotitic garnets

Experimental methods

Starting material

The starting material compositions are listed in Table 1. The starting compositions were constructed to obtain the olivine–garnet–orthopyroxene–clinopyroxene phase assemblage representative for the upper mantle. We reduced the olivine component compared to a typical mantle composition to increase the modal amount of garnet and orthopyroxene. To model different degrees of depletion of the mantle rock, we varied the Cr/(Al + Cr) of the bulk compositions between 0 < Cr/(Cr + Al) < 0.5. Two different relative amounts of garnet and pyroxene components are chosen to ensure that pyroxene is always present, even at high pressures and correspondingly high solid solution between garnet and pyroxene. As a starting material, we used either sintered oxide and carbonate mixtures, or glasses prepared from oxide mixtures. The oxides that were used are SiO_2, Al_2O_3, MgO, and Cr_2O_3, and for Ca, we used $CaCO_3$. MgO was fired at 1000 °C to release all absorbed hydroxides and carbonates and stored at 110 °C before use. All mixtures were homogenized in an agate mortar under acetone for approximately 45 min. For the compositions that were fused into a glass, the oxide powder was molten at 1600 °C in a platinum crucible, after which it was quenched, crushed, and homogenized again in a mortar. The melting procedure was performed twice. However, the starting compositions that were high in Cr_2O_3 have very high liquidus temperatures which made it impossible to prepare glasses without eskolaite (Cr_2O_3) crystals. Furthermore, we found that oxide starting materials are more likely to result in larger garnet crystals, probably because the presence of micron-sized particles of Al_2O_3 or Cr_2O_3 helps promote the nucleation of garnet. To further facilitate garnet growth and attainment of equilibrium in the experiments, some trace amounts of water were added to some of the starting composition in the form of brucite ($Mg(OH)_2$), (Table 2). For two reversal experiments, a starting material was prepared which is identical to the composition of the garnets from experiment mj7_6, a run which was performed at 12.5 GPa, 1500 °C (Tables 1, 3). The starting material was prepared from SiO_2, Al_2O_3, MgO, Cr_2O_3, $CaSiO_3$, and $Mg(OH)_2$ following the aforementioned procedures.

Oxygen fugacity buffer

In some initial experiments with the high Cr starting materials, we observed increased modal amounts of olivine, while no pyroxenes were present. This may be due to the presence of Cr^{2+}, which is known to stabilize olivine with respect to pyroxene (Li et al. 1995). In these cases, the garnet–pyroxene equilibrium is not attained, so these experiments are not suitable for our purpose. It has been suggested that at higher temperatures (>1500 °C), a

Table 1 Composition of starting materials

	mj2	mj3	mj4	mj5	mj6	mj7	rev
MgO	29.9	29.7	28.7	33.8	33.6	33.0	25.6
SiO_2	47.7	47.3	45.7	51.9	51.6	50.7	44.8
CaO	4.4	4.4	4.2	4.3	4.3	4.2	7.1
Cr_2O_3		2.7	13.0		2.0	7.2	12.5
Al_2O_3	17.9	15.9	8.4	10.0	8.6	4.9	9.9
total	100.0	100.0	100.0	100.0	100.0	100.0	100.0
Cr#[a]	0.0	0.10	0.51	0.0	0.13	0.50	0.46

[a] Cr# is Cr/(Cr + Al)

Table 2 Experimental results and conditions

Composition	Sample	Pressure (GPa)	*T* (°C)	Phases	Assembly
mj2	mj2_12[a]	6	1400	gt ol cpx opx	18/12
mj2	mj2_6[a]	9	1400	gt ol cpx opx	14/8
mj2	mj2_7[a]	9	1400	gt ol opx melt	14/8
mj2	mj2_4	6	1500	gt ol opx cpx	18/12
mj2	mj2_13	9	1500	gt ol cpx opx	14/8
mj2	mj2_14	9	1700	gt opx cpx melt	14/8
mj2	mj2_11	12	1700	gt ol	14/8
mj3	mj3_12[a]	9	1400	gt ol opx	14/8
mj3	mj3_1	6	1400	gt ol opx cpx	18/12
mj3	mj3_4	6	1500	gt ol opx cpx	18/12
mj3	mj3_7	9	1500	gt ol opx cpx	18/12
mj4	mj4_10[a,b]	9	1400	gt ol opx	14/8
mj4	mj4_13[b]	9	1600	gt ol opx cpx	14/8
mj4	mj4_6	9	1500	gt ol cpx	14/8
mj4	mj4_7	9	1700	gt ol cpx	14/8
mj4	mj4_11	11	1700	gt ol cpx	14/8
mj4	mj4.3	12	1700	gt ol	14/8
mj5	mj5_2[a]	11	1400	gt opx cpx	14/8
mj5	mj5_7[a]	12.5	1500	gt ol opx cpx	10/4
mj5	mj5_8[a]	14.5	1500	gt ol opx cpx	10/4
mj6	mj6_2[a]	9	1400	gt ol opx cpx	14/8
mj7	mj7_1[a]	11	1400	gt opx cpx	14/8
mj7	mj7_6[a,b]	12.5	1500	gt opx	10/4
mj7	mj7_7[a,b]	14.5	1500	gt ol opx	10/4
rev	rev1[a,b]	12.5	1650	gt st melt	14/8
rev	rev2[a,b]	9	1500	gt st opx cpx melt	14/8
rev	rev3[a,b,c]	12.5–9	1500	gt st opx cpx melt	14/8

gt garnet, *ol* olivine, *opx* orthopyroxene, *cpx* clinopyroxene, *st* stishovite

[a] Experiments containing water

[b] Experiments with Re–ReO_2 buffer

[c] Runtime is 24 h for all experiments except rev2 and rev3 which have run for 52 h

significant part of Cr may occur in the divalent state (Berry and O'Neill 2004). The potential presence of Cr^{2+} and the implications of that for phase stability are further discussed in the results section of this paper. In order to stabilize Cr^{3+} in our runs, we used the Re–ReO_2 solid-state oxygen fugacity buffer in the high Cr experiments, which is oxidizing enough to ensure that most of the Cr is in the trivalent state (Li et al. 1995; Berry and O'Neill 2004). Additionally, Re is very incompatible in garnet, pyroxene, and olivine so it is not expected to affect the stability of any of these minerals. The buffer was added as a sliver of Re metal at the top and/or the bottom of the capsule, together with a small amount of ReO_2 powder. The metal sliver helped to separate the ReO_2 oxide powder from the rest of the experimental charge, which was convenient because Re has a very high Z number which makes it uncomfortably bright in BSE images. We observed that reaction rims of ReO_2 oxide formed around the Re metal, which shows that the buffering reaction is indeed taking place. This approach seems to work: In buffered experiments, the modal abundance of olivine is decreased and pyroxene is present. However, the olivines sometimes still have high Cr content (see the analytical results section). In Table 2 is noted which of the experiments contain the fO_2 buffer.

Multi-anvil experiments

Most experiments were performed in a 1000-ton Walker-cell multi-anvil press at the Institute of Mineralogy at the University of Münster. One regular experiment (containing two samples: mj2_11 and mj4_3) and the two reversal experiments were performed at the Institute of Geochemistry and Petrology at ETH Zürich. Three different assemblies were used to cover the required range of pressures. For the lowest pressures (up to 6 GPa), an 18/12 (octahedron edge length/truncation edge length) ceramic-casted octahedron (Aremco 584 OF) was used. For the intermediate pressures (up to 12 GPa), we used a 14/8 assembly made from Cr-doped MgO and for the highest pressures (up to 14.5 GPa) a 10/4 assembly of the same material. The 18/12 casted assembly contains gaskets of the same material as the octahedron, and for the two other assemblies, we used pyrophyllite gaskets. For each experiment, the starting material is loaded into a noble metal capsule, either Pt or AuPd in the water-bearing experiments. The capsule is welded shut with a PUK 3 professional arc welder (Lampert Werktechnik GmbH, Germany), and then left in acetone for 2 h and weighted before and afterward to check for possible leakage. Depending on which multi-anvil assembly is used,

Table 3 Garnet compositions

Composition	mj2	mj2	mj2	mj2	mj2	mj2	mj3	mj3
Sample	Mj2_12	mj2_6	mj2_7	mj2_4	mj2_13	mj2_14	Mj3_12	mj3_1
Pressure (GPa)	6	9	9	6	9	9	9	6
T (°C)	1400	1400	1400	1500	1500	1700	1400	1400
n	12	24	37	6	9	8	13	21
MgO	26.8 ± 0.3	26.8 ± 0.4	26.9 ± 0.1	26.9 ± 0.2	28.3 ± 0.1	28.5 ± 0.2	26.8 ± 0.3	25.8 ± 0.2
SiO_2	44.9 ± 0.3	45.2 ± 0.2	45.2 ± 0.2	44.7 ± 0.2	46.0 ± 0.2	45.8 ± 0.3	44.4 ± 0.3	43.8 ± 0.2
CaO	4.5 ± 0.1	4.4 ± 0.3	4.2 ± 0.1	4.4 ± 0.1	3.9 ± 0.1	3.6 ± 0.2	4.6 ± 0.3	5.3 ± 0.2
Cr_2O_3							3.5 ± 0.9	4.2 ± 0.4
Al_2O_3	23.9 ± 0.2	23.8 ± 0.4	23.9 ± 0.2	23.5 ± 0.2	21.8 ± 0.3	22.1 ± 0.3	21.0 ± 0.4	20.9 ± 0.3
Total	100.1 ± 0.3	100.2 ± 0.2	100.1 ± 0.3	99.6 ± 0.3	100.1 ± 0.4	100.2 ± 0.3	100.2 ± 0.7	100.0 ± 0.3
Mg	2.71 ± 0.03	2.71 ± 0.04	2.71 ± 0.01	2.74 ± 0.01	2.86 ± 0.02	2.88 ± 0.02	2.74 ± 0.04	2.66 ± 0.02
Si	3.04 ± 0.01	3.06 ± 0.02	3.06 ± 0.01	3.05 ± 0.01	3.12 ± 0.01	3.10 ± 0.02	3.05 ± 0.01	3.03 ± 0.01
Ca	0.32 ± 0.01	0.32 ± 0.02	0.30 ± 0.01	0.32 ± 0.01	0.28 ± 0.01	0.26 ± 0.01	0.34 ± 0.02	0.39 ± 0.02
Cr							0.19 ± 0.05	0.23 ± 0.03
Al	1.91 ± 0.02	1.90 ± 0.03	1.91 ± 0.01	1.89 ± 0.01	1.75 ± 0.02	1.76 ± 0.02	1.70 ± 0.03	1.70 ± 0.02
Total	8.00 ± 0.01	7.99 ± 0.00	7.99 ± 0.01	8.00 ± 0.01	8.01 ± 0.01	8.01 ± 0.01	8.01 ± 0.01	8.01 ± 0.01
Composition	mj3	mj3	mj4	mj4_13	mj4	mj4	mj4_11	mj4
Sample	mj3_4	mj3_7	mj4_10	mj4_13	mj4_6	mj4_7	mj4_11	mj4_3
Pressure (GPa)	6	9	9	9	9	9	11	12
T (°C)	1500	1500	1400	1600	1500	1700	1700	1700
n	29	15	10	4	9	8	14	23
MgO	26.0 ± 0.2	27.0 ± 0.5	25.1 ± 0.3	25.8 ± 0.2	25.7 ± 0.5	25.8 ± 0.5	25.7 ± 0.3	25.9 ± 0.1
SiO_2	44.0 ± 0.3	45.0 ± 0.4	42.4 ± 0.3	43.1 ± 0.2	43.5 ± 0.4	43.1 ± 0.2	43.6 ± 0.3	44.2 ± 0.1
CaO	5.1 ± 0.2	4.7 ± 0.3	4.8 ± 0.3	4.5 ± 0.0	4.8 ± 0.3	4.8 ± 0.4	5.0 ± 0.4	5.0 ± 0.1
Cr_2O_3	4.4 ± 0.6	3.8 ± 1.1	15.6 ± 0.9	14.4 ± 0.2	14.9 ± 1.4	15.0 ± 0.3	14.3 ± 0.8	14.8 ± 0.2
Al_2O_3	20.3 ± 0.5	19.9 ± 0.7	12.0 ± 0.9	12.3 ± 0.3	11.4 ± 0.8	11.3 ± 0.2	11.3 ± 0.6	10.8 ± 0.2
Total	99.8 ± 0.3	100.2 ± 0.3	100.3 ± 0.4	100.5 ± 0.2	100.3 ± 0.3	99.9 ± 0.4	100.3 ± 0.4	100.8 ± 0.2
Mg	2.68 ± 0.02	2.76 ± 0.04	2.68 ± 0.02	2.74 ± 0.02	2.73 ± 0.04	2.75 ± 0.04	2.73 ± 0.03	2.74 ± 0.01
Si	3.05 ± 0.01	3.09 ± 0.02	3.04 ± 0.01	3.07 ± 0.01	3.10 ± 0.01	3.09 ± 0.01	3.12 ± 0.01	3.14 ± 0.01
Ca	0.38 ± 0.01	0.34 ± 0.03	0.37 ± 0.02	0.34 ± 0.00	0.37 ± 0.03	0.37 ± 0.03	0.39 ± 0.03	0.38 ± 0.01
Cr	0.24 ± 0.04	0.20 ± 0.07	0.89 ± 0.06	0.81 ± 0.01	0.84 ± 0.08	0.85 ± 0.02	0.81 ± 0.05	0.83 ± 0.01
Al	1.66 ± 0.04	1.61 ± 0.06	1.01 ± 0.07	1.03 ± 0.02	0.96 ± 0.07	0.95 ± 0.02	0.95 ± 0.05	0.91 ± 0.01
Total	8.01 ± 0.01	8.01 ± 0.01	8.00 ± 0.01	8.00 ± 0.01	8.00 ± 0.01	8.01 ± 0.00	8.00 ± 0.01	7.99 ± 0.01
Composition	mj5	mj5	mj5	mj6	mj7	mj7	mj7	
Sample	Mj5_02	mj5_07	mj5_8	mj6_2	mj7_1	Mj7_6	mj7_7	
Pressure (GPa)	11	12.5	14.5	9	11	12.5	14.5	
T (°C)	1400	1500	1500	1400	1400	1500	1500	
n	6	11	13	15	15	7	6	
MgO	27.6 ± 0.1	27.8 ± 0.3	29.0 ± 0.2	25.6 ± 0.5	24.3 ± 0.4	25.6 ± 0.9	24.9 ± 1.3	
SiO_2	45.8 ± 0.1	46.5 ± 0.3	48.8 ± 0.3	44.1 ± 0.3	43.8 ± 0.2	44.8 ± 0.4	45.7 ± 1.4	
CaO	4.5 ± 0.2	5.9 ± 0.2	6.5 ± 0.2	5.6 ± 0.4	7.0 ± 0.3	7.1 ± 1.1	9.1 ± 0.6	
Cr_2O_3				4.6 ± 2.2	14.0 ± 1.2	12.5 ± 2.2	12.4 ± 4.5	
Al_2O_3	21.8 ± 0.2	19.4 ± 0.3	15.7 ± 0.5	20.3 ± 1.9	11.2 ± 0.8	9.9 ± 1.6	7.7 ± 3.5	
Total	99.8 ± 0.2	99.8 ± 0.4	100.3 ± 0.3	100.2 ± 0.4	100.5 ± 0.1	100.6 ± 0.6	100.1 ± 0.3	

Table 3 continued

Composition	mj5	mj5	mj5	mj6	mj7	mj7	mj7
Sample	Mj5_02	mj5_07	mj5_8	mj6_2	mj7_1	Mj7_6	mj7_7
Pressure (GPa)	11	12.5	14.5	9	11	12.5	14.5
T (°C)	1400	1500	1500	1400	1400	1500	1500
n	6	11	13	15	15	7	6
Mg	2.80 ± 0.01	2.83 ± 0.03	2.95 ± 0.02	2.63 ± 0.04	2.59 ± 0.04	2.72 ± 0.10	2.68 ± 0.13
Si	3.12 ± 0.00	3.19 ± 0.01	3.33 ± 0.02	3.05 ± 0.02	3.13 ± 0.01	3.20 ± 0.02	3.29 ± 0.08
Ca	0.33 ± 0.01	0.43 ± 0.01	0.48 ± 0.02	0.41 ± 0.03	0.53 ± 0.03	0.55 ± 0.09	0.70 ± 0.05
Cr				0.25 ± 0.13	0.79 ± 0.07	0.71 ± 0.13	0.71 ± 0.27
Al	1.75 ± 0.01	1.57 ± 0.03	1.26 ± 0.04	1.65 ± 0.15	0.95 ± 0.07	0.83 ± 0.13	0.65 ± 0.29
Total	8.00 ± 0.01	8.03 ± 0.01	8.03 ± 0.01	8.00 ± 0.01	8.00 ± 0.01	8.03 ± 0.00	8.03 ± 0.01

Composition	rev	rev
Sample	rev1	rev3
Pressure (GPa)	12.5	9
T (°C)	1650	1500
n	17	18
MgO	26.4 ± 0.2	25.4 ± 0.8
SiO_2	44.6 ± 0.2	43.0 ± 0.3
CaO	5.3 ± 0.1	4.9 ± 1.0
Cr_2O_3	14.0 ± 0.4	16.2 ± 0.7
Al_2O_3	10.3 ± 0.2	10.9 ± 0.4
Total	100.7 ± 0.2	100.5 ± 0.3
Mg	2.79 ± 0.02	2.70 ± 0.08
Si	3.17 ± 0.01	3.08 ± 0.01
Ca	0.40 ± 0.01	0.37 ± 0.08
Cr	0.78 ± 0.02	0.92 ± 0.04
Al	0.86 ± 0.01	0.92 ± 0.03
Total	8.01 ± 0.005	8.00 ± 0.01

Uncertainties are given as 1σ standard deviation

either one or two capsules were loaded into the octahedron. As a heater, we used a graphite heater for pressures up till 6 GPa, and $LaCrO_3$ heaters at higher pressures, a stepped heater for the two larger assemblies, and a straight heater in the 10/4 assembly. Experiments are brought up to pressure at a rate of ~60 to 100 tons per hour. The temperature was increased to the desired run temperature at a rate of ~50 °C per minute. Run temperatures were measured and controlled with a W–Re (type C) thermocouple, together with a Eurotherm temperature controller. In the 18/12 and 14/8 assemblies, the thermocouple is inserted from the top inside the furnace, parallel to its axis, at ~0.5 mm distance from the capsule. In the 10/4 assembly, the thermocouple is inserted radially, through the octahedron center, between the two capsules (as described in Stewart et al. 2006). The run times were typically 24 h (Table 2). The overall temperature uncertainties including temperature fluctuations and thermal gradients are about 20 °C for 18/12 and 14/8 assemblies and about 50 °C for the 10/4 assembly. After the experiment, the samples were quenched by turning of the power to the heater, which leads to a rapid decrease in temperature to below 500 °C in less than a second.

Multi-anvil pressure calibration

The different assemblies were calibrated for pressure against solid-state mineral phase transformation. For the 18/12 and the 14/8 assemblies, a room-temperature calibration was performed, using the Bismuth I–II and IV/V phase transformations at 2.55 and 7.7 GPa, respectively (Degtyareva et al. 2004). At higher temperatures, we used the phase transformations quartz–coesite (3.0 GPa, 1100 °C), $CaGeO_3$ garnet to perovskite (6.0 GPa, 1100 °C), and (only for the 14/8 assembly) coesite–stishovite (9 GPa, 1100 °C) (Susaki et al.

1985; Bose and Ganguly 1995; Zhang et al. 1996). The 10/4 assembly was calibrated against the transition of olivine to wadsleyite at 14 GPa and 1400 °C (Frost 2003).

Analytical methods

The major element analyses were performed with a JEOL JXA-8900 M electron microprobe analyzer (EPMA), at the University of Münster, Germany. The reversal experiments rev1, rev2, and rev3 were measured with a JEOL JXA-8200 EPMA at the Institute of Geochemistry and Petrology at ETH Zürich, Switzerland. All mineral phases were analyzed with a focused beam (1–2 μm beam diameter), a beam current of 15 nA, and an acceleration voltage of 15 kV. Counting times were 20 s on the peak and 10 s on the background. For the garnet measurements, the standard materials that were used are grossular or grossular-rich garnet (Ca), pyrope (Mg, Si, Al), and synthetic eskolaite (Cr_2O_3) or chromite (Cr). For all other silicate measurements, we used synthetic eskolaite (Cr), hypersthene (Si), kyanite (Al), diopside (Ca), and olivine (Mg). A number of secondary reference materials, i.e., several natural garnets and the other minerals (diopside, Cr-diopside, chromite, and olivine), were measured as unknowns to monitor external precision and accuracy. The major element data for garnet are presented in Table 3, and for the other minerals (olivine, opx, cpx) in the electronic appendix (Table 6). The individual measurements of reversal experiment rev2 are listed in Table 7 of the electronic appendix.

For determining the majorite content of natural and experimentally grown garnet, it is very important to obtain as accurate and precise microprobe measurements as possible, because a small difference in SiO_2 leads to a significantly different majorite content. Therefore, measurements that deviate from the ideal totals of 100 by more than ±1.0 or total cation sum of 8.00 by more than ±0.02 were generally discarded. All data satisfying these quality control criteria were subsequently averaged. We only used analyses which were not compromised by inclusions or neighboring crystals. EPMA measurements were repeated on a number of samples on different measuring days to test reproducibility; these measurements always returned identical results within the analytical uncertainties.

Results

Experimental results

After the experiment, each sample was mounted in an epoxy resin, polished, and investigated by optical microscopy and studied using scanning electron microscopy (SEM). Figure 3a–f shows the backscatter electron images (BSE) of some representative samples. All experimental run products contain garnet. Most runs also contain pyroxene, typically both orthopyroxene (opx) (or at high pressure, Ca-poor clinoenstatite) and (Ca-rich) clinopyroxene (cpx) but in some cases only one of the two pyroxenes. The Cr-free compositions always contain opx and most of them also cpx, while the Cr-rich compositions sometimes only contain cpx. Most run products also contain olivine. The experimental run conditions and phases present in the experiments are given in Table 2. Many experiments contained only very small crystals (<5 microns) and could therefore not be measured properly and were discarded. For a successful microprobe analysis in our study, we found that it is important that crystals are at least 5–10 microns in size. When the crystals are smaller, the risk of contamination or overlap analysis from a nearby crystal, e.g., a small garnet next to a pyroxene, may lead to an erroneously high SiO_2 concentration in garnet which could be misinterpreted as a high majorite content.

Attainment of equilibrium

Attainment of equilibrium in the experiments needs to be assessed carefully, as garnet is well known to react sluggishly in subsolidus experiments (e.g., Klemme and O'Neill 1997, 2000b; Klemme 2004; Brey et al. 2008). Experiments in a Cr-containing system are also well known to be slow to equilibrate (Doroshev et al. 1997; Girnis et al. 2003; Klemme and O'Neill 2000b). For this reason, some of the initial experiments were not fully equilibrated. This was obvious from (sometimes patched) zonation in the garnets in some experiments, or (slightly) non-stoichiometric compositions of the garnets. These experiments were not further investigated. By adding some water to the experiments as flux, the garnet-forming reaction was enhanced. This resulted in the growth of larger and more homogeneous garnet and pyroxene crystals.

We assumed that the experiments are fully equilibrated when the following conditions are met: (1) The garnets are not zoned, (2) the garnets show a (near) euhedral crystal shape, and (3) the microprobe measurements yield a stoichiometric garnet composition.

To further assess whether equilibrium has been obtained in our experiments, we performed a two-step reversal experiment. We used a starting composition identical to the garnet composition of experiment mj7_6, which was performed at 12.5 GPa. As the first step, two capsules (rev1 and rev2) with this starting composition were run at 12.5 GPa and 1650 °C for 24 h. One capsule (rev2) was then recovered and run again without opening at 9 GPa and 1500 °C for 52 h, together with another capsule (rev3) containing unreacted starting material. Sample rev1 contains garnet, stishovite, and a hydrous silicate melt. The

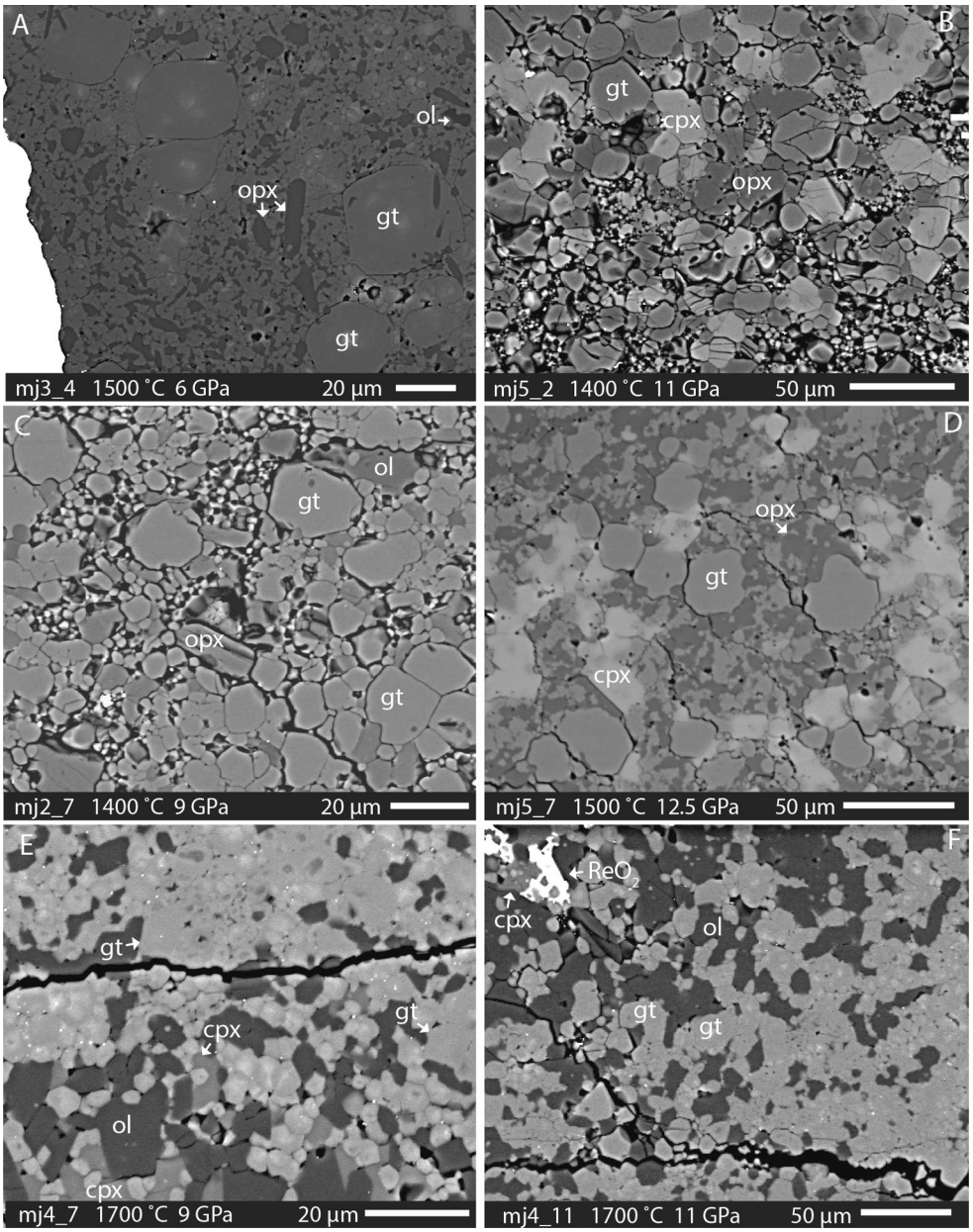

Fig. 3 Backscatter SEM images of six of the samples. Gt stands for garnet, ol for olivine, opx for orthopyroxene, and cpx for clinopyroxene. In a (mj3_4), 3e (mj4_7), and 3f (mj4_11), some garnets show some patchy zoning, but other garnets in the same sample are homogeneous. In f, some ReO_2 is visible in the image (*white*); this is the oxygen fugacity buffer that was added to some of the samples

garnet is homogeneous, and very similar in composition to the garnets of mj7_6 and has identical majorite content within analytical uncertainties. Samples rev2 and 3 both contain garnet, stishovite, orthopyroxene, clinopyroxene, and minor amounts of hydrous silicate melt. Rev3 contains homogeneous garnets that are similar in composition and majorite content to the other Cr-rich 9 GPa experiments.

Sample rev2, the sample which has first been run at 12.5 GPa and then at 9 GPa, has not fully re-equilibrated to the 9 GPa conditions. Instead, it contains garnets with Si contents gradually increasing from 3.06 (most likely the equilibrium composition at 9 GPa) up to 3.20 (in equilibrium at 12.5 GPa). Some of the garnets start to show exsolution of pyroxene and SiO_2.

The reversal runs show that synthesis experiments using oxide mixtures are the best way to achieve equilibrated minerals in these bulk compositions, as reaction rates in experiments with pre-synthesized minerals, such as in the reversal experiments, are just too slow to allow for equilibration in typical timescales of multi-anvil experiments.

Equilibrium between garnet and pyroxene

In order to determine the pressure effect on the majorite substation in garnet, it is important that the silica activity ($aSiO_2$) in the experiment is controlled by the presence of pyroxene and olivine. As majoritic garnet is essentially a solid solution between garnet and pyroxene, an absence of pyroxene in the sample means that the majorite content will not increase with pressure. If experiments do not contain pyroxenes in equilibrium with garnet, the majorite content depends only on the bulk composition of the sample and not necessarily on pressure. These experiments are therefore not appropriate for geobarometry based on majorite component in garnet. We assume that it makes no difference whether the garnet is in equilibrium with opx (at pressure >10 GPa low-Ca clinopyroxene) or (high Ca) cpx. Draper et al. (2003a, b) suggested that garnet in the presence of opx may have a higher majorite content compared to garnet in present with cpx; however, in our experimental dataset, we see no evidence for this. Some of our experiments did not contain any pyroxene, due to the high pressure and correspondingly high majorite content, or because of the presence of Cr^{2+}, which stabilized olivine in respect of pyroxene. These experiments are not further investigated, except for two samples from one experiment (mj4_3 and 2_11). In those two experiments, judged by the measured majorite content combined with the pressure of that experiment (12 GPa), we can assume that the conditions of the experiment are very close to the pyroxene-out reaction, and therefore, the majorite component will still be fairly representative for that pressure. For the geobarometer (see below), it does not make any difference whether or not these two experiments are included.

Analytical results

Garnet

The composition of all garnets in our experiments can be described as a solid solution between the garnet end member pyrope ($Mg_3Al_2Si_3O_{12}$), knorringite ($Mg_3Cr_2Si_3O_{12}$), majorite ($Mg_4Si_4O_{12}$), and a minor grossular component ($Ca_3Al_2Si_3O_{12}$), see Table 3 and Fig. 4. The SiO_2 content ranges from 42.2 to 48.9 wt%, increasing with pressure (Fig. 5c). The Al_2O_3 content depends on the starting material, and the experiments with higher Cr/(Cr + Al) content yield lower Al_2O_3 garnets as Al competes with Cr for the octahedral site. Al_2O_3 in garnet decreases with pressure, because 2 Al^{3+} are replaced by Si^{4+} + Mg^{2+} on the octahedral site and the molar amount of majorite component increases. Similar to Al_2O_3, the Cr_2O_3 content also depends on the starting material (12.4–15.6 wt% Cr_2O_3 for the high Cr compositions, 3.5–4.6 wt% Cr_2O_3 for the low Cr compositions (Fig. 5a). The Cr-containing garnets are sometimes slightly zoned in Cr–Al. The MgO content of garnet ranges from 24 to 29 wt%, and CaO from 3.6 to 9.10 wt%. In the high Cr experiments, CaO is higher and MgO is lower compared to the Cr-free experiments. Both MgO and CaO also slightly increase with increasing pressure. The increase in MgO with increasing majorite content is due to the coupled substitution of 2 Al^{3+} with one 1 Si^{4+} and 1 Mg^{2+} (see Eq. 1). Ca^{2+} is not expected to partition into the octahedral site due to the size mismatch, so the increase in CaO is due to an exchange of Ca and Mg on the dodecahedral site instead. The majorite content in our garnets shows a gradual increase with pressure (Fig. 6a). The high Cr compositions yield garnets with a lower majorite content at a given pressure. To investigate the effect of temperature, we compare a series of experiments at one pressure (9 GPa), with temperatures increasing from 1400 to 1700 °C. For this range of temperatures, the majorite content of the garnets is within the error of each other (Fig. 6b). This implies that the temperature effect on the majorite forming reaction is negligible.

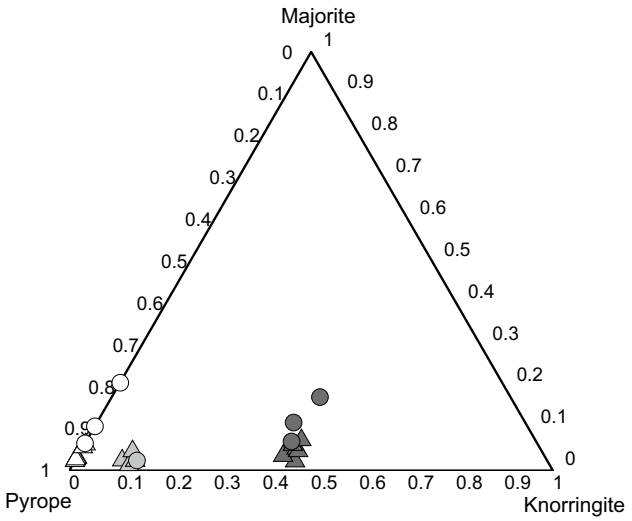

Fig. 4 Compositions of the garnets in a ternary diagram with the end member pyrope ($Mg_3Al_2Si_3O_{12}$), knorringite ($Mg_3Cr_2Si_3O_{12}$), and majorite (in this diagram shown as $Mg_4Si_4O_{12}$). The *white symbols* depict the Cr-free compositions; the *light gray* symbols show the compositions with ~5 wt% Cr and the *dark gray symbols* with ~15 wt%. The *triangle symbols* represent the low SiO_2 compositions (Mj2, Mj3, Mj4) and the *circles* the high SiO_2 compositions (Mj5, Mj6, Mj7)

Pyroxenes

Orthopyroxene (or clinoenstatite at higher pressures) compositions do not vary much between different experiments. The MgO content varies between 35.5 and 40.3 wt%, SiO_2 between 57.4 and 59.4 wt%, CaO between 0.2 and 2.6 wt%,

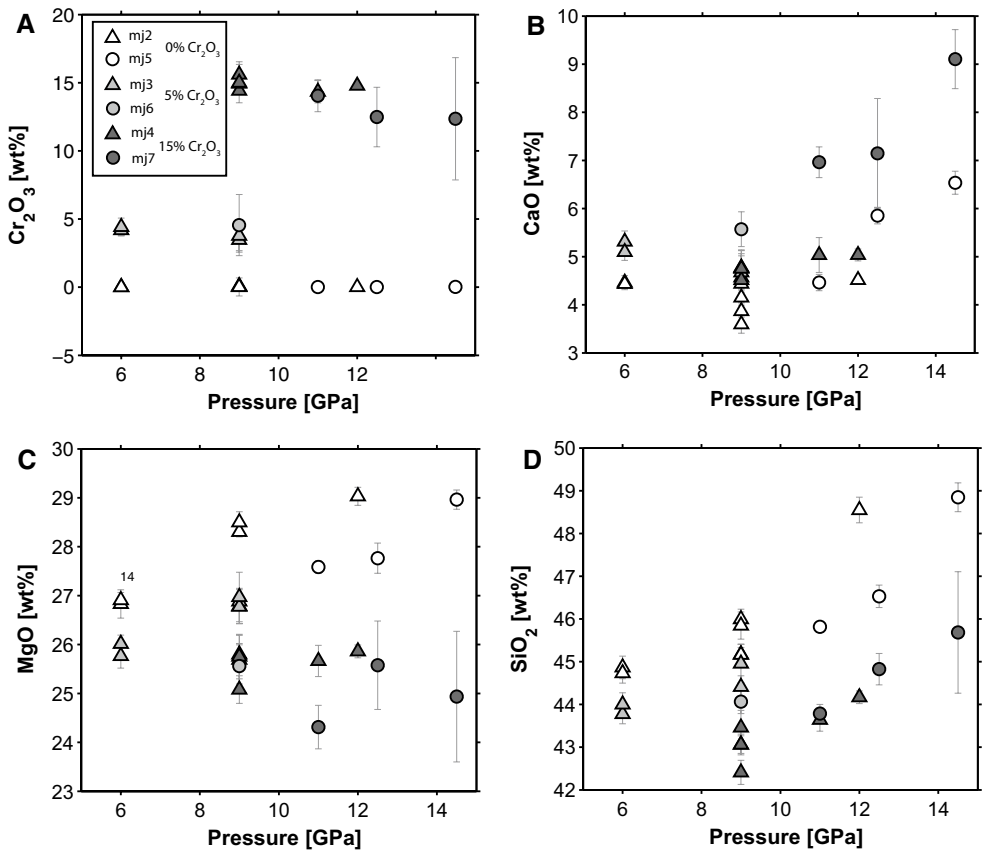

Fig. 5 **a** Cr_2O_3 content of the garnets versus pressure (GPa). **b** CaO content versus P, **c** MgO content, and **d** SiO_2 content

Al_2O_3 between 0.15 and 1.9 wt%, and up to 2.3 wt% Cr_2O_3 for the high Cr compositions (Table 6 electronic appendix).

Clinopyroxene shows a wider range of compositions, as well as a large difference in modal abundance between the experiments. In most runs, there are only a few cpx crystals present, but in the charges with high bulk Cr, cpx is sometimes the only pyroxene present and its modal abundance is higher. The MgO content of cpx ranges from 20.2 to 31.8 wt%, the SiO_2 content from 53.1 to 57.1 wt%, Al_2O_3 ranges from 0.4 and 5.3 wt%, and the Cr_2O_3 content varies between 0 and 3.9 wt%. The CaO content varies a lot between the experiments with different bulk compositions: from 7.7 to 23.1 wt%. CaO is lowest for the experiments with high Cr composition, when the modal cpx abundance is the highest.

Olivine

All olivines are nearly pure forsterites, with SiO_2 ranging from 41.5 to 43.7 wt% and MgO from 54.2 to 56.8 wt%. The olivines contain minor amounts of CaO (0.05–0.35 wt%), Al_2O_3 (0.02–0.3 wt%), and Cr_2O_3 in the Cr-bearing experiments (up to 1.0 wt%). As Cr^{3+} is incompatible in olivine due to the charge and size mismatch, the unexpectedly high Cr concentrations in olivine indicate that some Cr^{2+} may be present in the experiments. Some experiments with high Cr content contained an unexpectedly large amount of olivine, while pyroxene was absent. Since Cr^{2+} is not very compatible in garnet or pyroxenes, it may be that the presence of Cr^{2+} increases the stability of olivine, at the expense of pyroxene. When experiments were performed with the oxidizing solid-state Re–ReO_2 buffer, the modal amount of olivine decreased and pyroxene was present. However, the Cr_2O_3 content in these olivines was sometimes still high in these experiments (Table 6 electronic appendix). From this, it follows that high Cr concentrations in olivine do not necessarily indicate whether or not Cr^{2+} was present in any of the experiments, but the decrease in the modal amount of olivine in the fO_2-buffered experiments suggests this might be the case.

Discussion

A new geobarometer based on the majorite component in garnet

The aim of this study was to investigate and quantify the effect of composition and temperature on the stability of

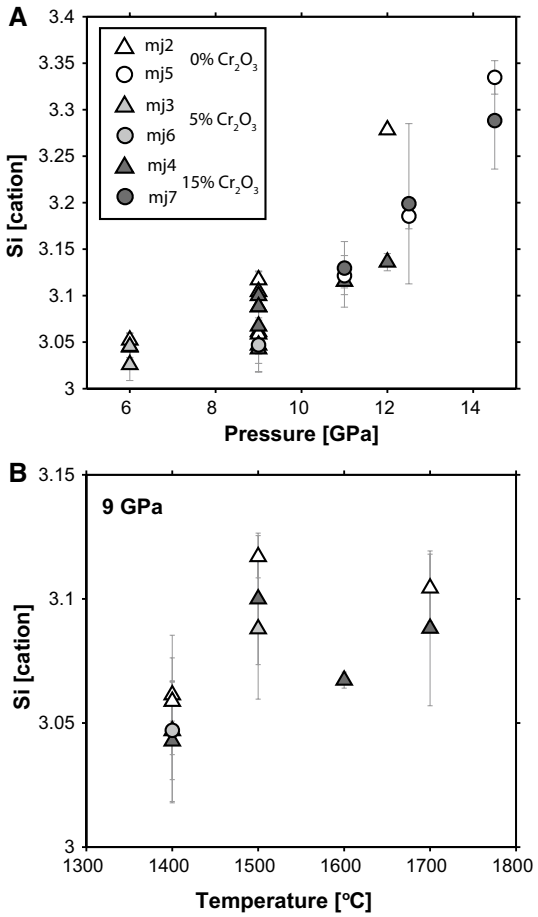

Fig. 6 **a** Majorite content (Si cation content > 3.00, with a total of 12 oxygen) of the garnets plotted against pressure. There is an obvious increase in majorite content with pressure. **b** Majorite content of all experiments performed at 9 GPa, plotted against temperature. There is no clear correlation between temperature and majorite content

the majorite component in garnet. To process the experimentally derived data presented above, we used a least squares fitting routine (MATLAB and Curve Fitting Toolbox; R2013a, The MathWorks) to fit our new data combined with the literature data to derive an empirical relation that may be used to estimate the pressure from the composition of a naturally occurring majoritic garnet.

When selecting the literature data to use for the fitting procedure, it is important to evaluate the quality of the experimental and analytical data, and whether the data are appropriate for our purpose. For selecting appropriate high-quality data from the literature, we use the same criteria as for our own EPMA measurements (total = 100 ± 1.0 wt%; sum of cations = 8 ± 0.02), as described in the analytics section. We made certain to only use the experiments where both garnet and pyroxene were present, as explained in the "Equilibrium between garnet and pyroxene" section. We did not use experimental results from papers where the majorite content of the garnets shows a wide range of majorite contents among runs that were performed at identical pressures and bulk compositions, as we consider this variation as indicative for either analytical issues or a lack of equilibration between the mineral phases. We also excluded experimental results from studies where the compositions of the garnets are close to end member majorite (i.e., Si cation content >3.9), because when reaching the majorite end member of the garnet solid solution, the majorite content no longer depends on pressure. The studies from which the garnet experiments did not meet all these criteria (e.g., Herzberg and Zhang 1996; Hirose 2002; Kawamoto 2004; Kesson et al. 1994; Kiseeva et al. 2013a, b; Litasov and Ohtani 2005; Ohtani et al. 1989; Ulmer and Sweeney 2002; Wang and Takahashi 2000; Thomson et al. 2016) were therefore not used to calibrate our barometer. The dataset used for the majorite barometers is presented in Table 9 of the electronic appendix.

We treated the dataset using a least squares fitting routine in MATLAB. This resulted in two different equations, one suitable for peridotitic compositions (Eq. 2), and one for eclogitic compositions (Eq. 3). Details of the fitting procedures (covariation and correlation matrices and *p* values) are given in the electronic supplements in this paper (Table 7). We found that in peridotitic compositions, the Si and Cr cation concentrations in garnet were the most important parameters that described the pressure dependency. As mentioned above, temperature has negligible effect on majorite substitution, which is encouraging for geobarometry. To derive Eq. 2, we used our new data in combination with experimental results from Akaogi and Akimoto (1977), (1979), Irifune (1987), and Walter (1998) (Fig. 7). For Eq. (3), we used the same data and added experimental results in eclogitic bulk compositions (Yasuda et al. 1994; Ono and Yasuda 1996; Wang and Takahashi 2000; Nishihara and Takahashi 2001; Gasparik 2002; Zhang et al. 2003; Okamoto and Maruyama 2004; Bobrov et al. 2008; Dymshits et al. 2013). The R^2 value (which stands for the goodness of the fit) of Eq. 3 is somewhat lower compared to Eq. 2 (R^2 for Eq. 2 = 0.94, R^2 = 0.83 for Eq. 3). We believe this is because the dataset for the Eq. 3 is substantially larger and also exhibits much more scatter between the different studies.

The empirical geobarometer for majoritic garnets in peridotitic compositions

$$P = a + b \times Si + c \times Cr \quad (2)$$

The empirical geobarometer for majoritic garnets in eclogitic compositions

$$P = a + b \times Si + d \times Na + e \times Ca \quad (3)$$

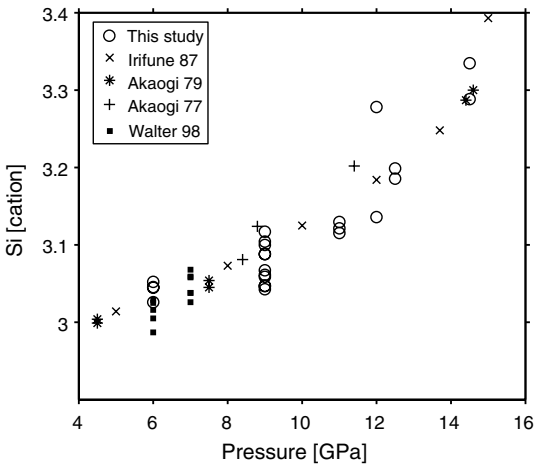

Fig. 7 Majorite content of the garnets of our study (*circles*) against pressure, compared with peridotitic garnets from the literature (Akaogi and Akimoto 1977, 1979; Irifune 1987, and Walter 1998). These data are used for the fitting procedure of Eq. 2

The fit parameters *a*, *b*, *c*, *d*, and *e* are shown in Table 4. Si, Cr, Na, and Ca stand for the cations per formula unit garnet, normalized to 12 oxygens.

The geobarometer for majorite garnets in peridotite compositions (Eq. 2) reproduces our data and the other experimental data very well. If we compare calculated pressures with experimental pressures, we find that the experimental data are reproduced within 12 % (root mean square error, see Tables 4, 8a). If we compare calculated results from Eq. 3 with experimental data for eclogitic garnets, we find that the experimental data are reproduced within 29 % (Fig. 8b). Especially at lower pressures (<8 GPa), Eq. 3 becomes less accurate. Our own (peridotitic) experimental data are reproduced reasonably well by Eq. 3; however, we find that the pressure is slightly overestimated at low pressures, while the pressures are underestimated at higher pressures. In Fig. 8b, we compare our barometer for eclogitic compositions to the barometer of Collerson et al. (2010). The pressures of all experiments used for our barometers, calculated according to the equation of Collerson et al. (2010), are depicted in Fig. 8b. It is clear that especially at high pressure, the calculated pressures deviate significantly from the experimental pressures.

In summary, we recommend to use Eq. (2) for majoritic garnets in peridotitic compositions and to use Eq. (3) for majoritic garnets in eclogitic compositions. If the lithology of the garnet is unknown, we recommend the use of Eq. 3. Caution should be used when using Eq. 3 at pressures for Si contents lower than 3.10.

The barometers are calibrated for pressures up to 15 GPa (Eq. 2) and 21.5 GPa (Eq. 3). However, it should be noted that, in the mantle, the maximum majorite content for a given pressure will only be reached if the Si activity is sufficiently high enough. This may not be the case at high pressures (above ~15 GPa) where no pyroxene is left in the mantle. The calculated pressure based on the majorite content will therefore always be the minimum pressure for a particular majoritic garnet inclusion.

Implication for naturally occurring majoritic garnets

Our empirical barometers can be used to estimate the pressures of formation or equilibration of naturally occurring majoritic garnets. In the introduction section, we briefly touched on the fact that majoritic garnets with peridotitic compositions are relatively scarce. However, several of those garnets were reported in the literature (Stachel 2001; Collerson et al. 2010 and references therein; Moore and Gurney 1989; Sobolev et al. 1997; Hutchison 1997; Sobolev et al. 2004; Pokhilenko et al. 2004; Banas et al. 2007; Moore and Gurney 1985; Stachel and Harris 1997; Tappert et al. 2005; Meyer and Mahin 1986). We summarized the literature results in Table 5. We used our geobarometers to determine the pressure of equilibration of these garnets. For comparison, we also list some eclogitic garnets (from the previously mentioned references). The average pressure of the peridotitic garnets is 10.0 GPa (with a standard deviation of 2.4), with the lowest pressure of 6.9 ± 0.8 GPa and the highest pressure at an amazingly high value of 15.0 ± 1.8 GPa.

To demonstrate the effect of Cr on the majorite content, we compare the pressures calculated for three different majoritic garnets: the sample with the highest pressure (yum-27 from Yakutia, Russia; Sobolev et al. 2004), the sample with the highest Cr content (G303-305h from Birim, Ghana; Stachel and Harris 1997), and an "average" peridotitic sample (a3-01 from Monastery, South Africa; Moore and Gurney 1985). The Si cation content of these garnets is 3.29, 3.06, and 3.13, respectively. Using Eq. 2, we calculate the pressure for yum-27 to 15 ± 1.8 GPa, while a garnet with the same majorite content but no Cr would yield a pressure of 13.9 ± 1.7 GPa. For G303-305h,

Table 4 Fit parameters

	a	*b*	*c*	*d*	*e*	R^2	RMSE
Equation 2	−77.1 ± 6.9	27.6 ± 2.2	1.67 ± 1.0			0.94	0.12
Equation 3	−29.6 ± 5.3	11.8 ± 1.6		7.81 ± 2.42	4.49 ± 0.88	0.83	0.29

Uncertainties are given as the 95 % confidence interval. RMSE is root mean square error

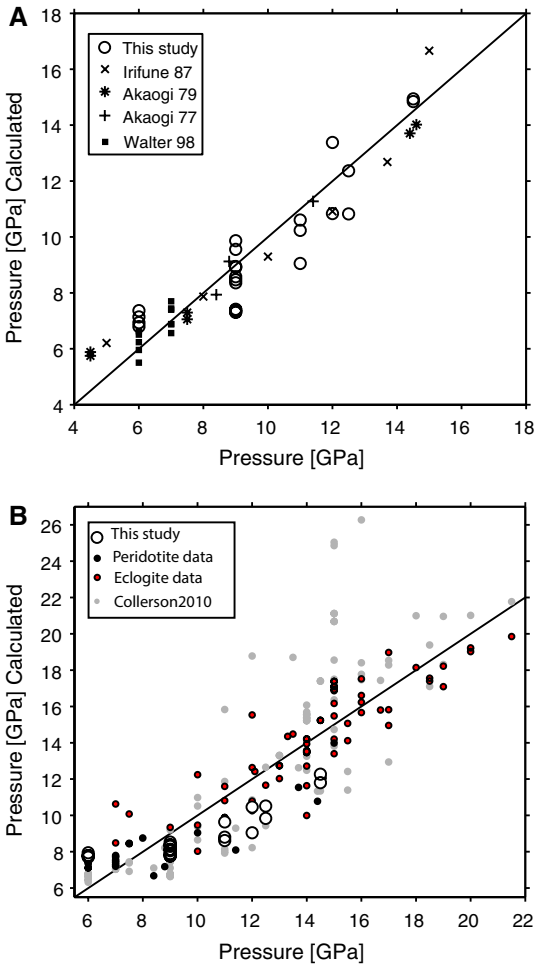

Fig. 8 **a** Pressures of the experiments (our data and literature data for peridotitic compositions, see Fig. 7) plotted against the calculated pressures using Eq. 2. The *black line* is the identity line (x = y). All peridotite data plot close to this *line*, which shows that the fit function is fairly accurate. **b** Experimental pressures compared with the calculated pressures (Eq. 3) of garnets from our study (*white circles*), peridotitic garnets (used for the calibration of Eq. 2) in *black dots* and eclogitic garnets (used for the calibration of Eq. 3) in *red dots*. The pressures calculated according to the fit function of Collerson et al. (2010) are shown in *gray circles*

the pressure is 9.6 ± 1.1 GPa while a Cr-free garnet would yield a pressure of 7.5 ± 0.9 GPa, and for a3-01, the pressure is 10 ± 1.2 GPa while a Cr-free garnet would have a pressure of 9.5 ± 1.1 GPa. This clearly shows that Cr has a significant effect on garnet stability, shifting the majorite substitution to higher pressures.

When we compare the eclogitic garnets with peridotitic garnets, the eclogitic garnets will have a higher majorite content at the same pressures, and this effect is especially seen at high pressure. As an example, consider the eclogitic garnet with the highest pressure in Table 5 (JF-22 from Jagersfontein; Tappert et al. 2005) has a Si cation content of 3.55 which corresponds to a pressure of 15 GPa, while the peridotitic sample yum-27 from Yakutia (Sobolev et al. 2004) also equilibrated at 15 GPa, but with much lower Si cation content (3.29). This demonstrates the importance of bulk composition on majorite geobarometry.

Implications for mantle mineralogy

Our geobarometers show that the majorite content in garnet depends mainly on pressure, but also on the composition of the garnet. This has implications for the phase relations in the upper mantle. At the same depths, garnets with a high Cr content will have a lower majorite content compared to garnets with low Cr, which indicates that the Cr-rich majoritic garnets that were reported in the literature (for references, see Table 5) must therefore come from very deep in the mantle. This also suggests that the rare high Cr majoritic garnets (e.g., Stachel 2001) are very significant as they indicate the presence of depleted, Cr-rich peridotite deep within the asthenospheric upper mantle or even in the transition zone.

In a "pyrolite" mantle composition (Green and Falloon 1998), the modal abundance of garnet increases significantly with increasing pressure up to ~40 vol% at 15 GPa (Frost 2008). In rocks with such high garnet contents, one would not expect high-Cr garnets to exist, simply because the Cr content of the garnets would be diluted. This implies that the high-Cr majoritic garnets discussed above must come from unusual, depleted mantle lithologies. One possibility is that these garnets come from parts of the mantle with extremely low modal garnet content, e.g., dunite that consists almost entirely of olivine or its high-pressure polymorphs. If these dunites contain some pyroxene component, to account for the majorite formation, and very low garnet modes, the Cr content in garnet could potentially be very high because most of the Cr in the rock will partition into the garnets. The low garnet abundance in these rocks but also the scarcity of dunite in the deep asthenospheric mantle may contribute to the relative scarcity of these garnets as diamond inclusions. Another possibility, of course, is that locally in the deep mantle depleted harzburgite exists with very high Cr/(Cr + Al). Overall, however, the occurrence of Cr-rich majoritic diamond inclusions is an important indicator that depleted lithosphere is subducted deep into the asthenospheric mantle and stays unmixed before the garnets are surrounded by a growing diamond. Note that the recent discovery of diamonds in Cr-spinels (Yang et al. 2007, 2014) from ophiolites in China also implies rapid subduction of Cr-spinels deep into the asthenospheric mantle before they are transported back to the surface. This could be a mechanism to introduce high-Cr/(Cr + Al) rocks into the asthenosphere, from which also the high-Cr majoritic garnets could originate.

It should be noted that while high-Cr garnets with a majorite component are relatively rare, low-Cr garnets of

Table 5 Majorite data from the literature

Reference source	1	2	2	3	4	5	5	6
	Monastery	Arkhangelsk	Arkhangelsk	Sao Luiz	Yakutia	Snap Lake	Snap Lake	Buffalo hills
	Kaapvaal craton	Baltic shield	Baltic shield	alluvial	Siberian craton	Slave craton	Slave craton	Buffalo head terrane
Sample name	a3-01	#2/13j	po-99	BZ237C	Yum-27	Sl3-31	Sl3-30	A209
(a) Peridotitic								
SiO_2	43.8	43.2	44.9	43.5	42.8	42.2	42.3	43.9
TiO_2	0.51	0.02	0.71	0.0	0.33	0.19	0.06	0.1
Al_2O_3	16.19	20.4	16.6	21.1	6.79	12.3	9.46	13.00
Cr_2O_3	5.34	3.0	1.23	3.0	10.2	11.8	12.8	6.32
FeO	7.23	5.8	8.65	6.0	5.67	6.52	7.64	8.43
MnO	0.27	0.23	0.21	0.9	0.28	0.32	0.33	0.29
MgO	22.9	24.1	23.5	22.3	12.2	21.1	21.2	22.00
CaO	3.66	2.94	3.77	1.7	20.8	4.68	5.11	5.34
Na2O	0.07	0.05	0.25	0.3	0.04	0.03	0.01	0.24
total	99.9	99.74	99.82	98.8	99.11	99.1	99	99.62
Si	3.13	3.05	3.20	3.09	3.29	3.11	3.17	3.20
Ti	0.03	0.001	0.04	0.001	0.02	0.01	0.003	0.01
Al	1.37	1.70	1.39	1.76	0.62	1.07	0.83	1.12
Cr	0.30	0.17	0.07	0.17	0.62	0.69	0.76	0.36
Fe	0.43	0.34	0.52	0.36	0.37	0.40	0.48	0.51
Mn	0.02	0.01	0.01	0.05	0.02	0.02	0.02	0.02
Mg	2.44	2.53	2.50	2.36	1.41	2.32	2.37	2.39
Ca	0.28	0.22	0.29	0.13	1.72	0.37	0.41	0.42
Na	0.01	0.01	0.03	0.04	0.01	0.004	0.001	0.03
Total	8.01	8.03	8.05	7.96	8.07	8.00	8.04	8.07
Pressure (GPa)[a]	10.0	7.3	11.4	8.6	15.0	10.1	11.7	12.0

Source	7	8	8	9	9	9	10	10
Mine	Jagersfontein	Birim	Birim	Premier	Monastery	Premier	Droujba	Droujba
Craton	Kaapvaal craton	West African craton	West African craton	Kaapvaal craton	Kaapvaal craton	Kaapvaal craton	West African craton	West African craton
Sample name	JF-43	G303-305 h	G204-206 h	P-98 g	Al-15d	P-50 g	#9i	#10i
SiO_2	43.2	40.8	41.9	41.8	46.3	44.0	43.2	44.0
TiO_2	0.53	0.02	0.61	0.11	1.05	0.07	0.69	0.34
Al_2O_3	16.1	7.0	19.52	15.5	13.6	19.23	19.9	21.3
Cr_2O_3	3.47	20.56	1.9	10.2	1.2	2.75	2.18	0.83
FeO	11.7	6.73	11.8	5.7	9.07	5.63	8.11	7.62
MnO	0.39	0.29	0.27	0.28	0.23	0.21	0.24	0.38
MgO	20	22.7	19.5	22.5	23.6	24.9	22.7	21.3
CaO	3.89	1.57	3.91	3.26	5.16	1.9	4.37	4.12
Na_2O	0.12	0.11			0.14		0.06	0.12
Total	99.4	99.78	99.44	99.35	100.35	98.69	101.45	100.01
Si	3.16	3.06	3.05	3.04	3.30	3.12	3.04	3.10
Ti	0.03	0.001	0.03	0.01	0.06	0.00	0.04	0.02
Al	1.39	0.62	1.67	1.33	1.14	1.61	1.65	1.77
Cr	0.20	1.22	0.11	0.59	0.07	0.15	0.12	0.05
Fe	0.72	0.42	0.72	0.35	0.54	0.33	0.48	0.45
Mn	0.02	0.02	0.02	0.02	0.01	0.01	0.01	0.02
Mg	2.18	2.54	2.12	2.44	2.51	2.63	2.38	2.24

Table 5 continued

Source	7	8	8	9	9	9	10	10
Mine	Jagersfontein	Birim	Birim	Premier	Monastery	Premier	Droujba	Droujba
Craton	Kaapvaal craton	West African craton	West African craton	Kaapvaal craton	Kaapvaal craton	Kaapvaal craton	West African craton	West African craton
Sample name	JF-43	G303-305 h	G204-206 h	P-98 g	Al-15d	P-50 g	#9i	#10i
Ca	0.30	0.13	0.31	0.25	0.39	0.14	0.33	0.31
Na	0.02	0.02			0.02		0.01	0.02
Total	8.02	8.02	8.02	8.00	8.05	8.00	8.05	7.98
Pressure (GPa)[a]	10.6	9.6	7.3	7.8	14.3	9.3	6.9	8.7

Source	4	4	5	5	7	7	7	7	7	7
Mine	Yakutia	Yakutia	Snap Lake	Snap Lake	Jagersfontein	Jagersfontein	Jagersfontein	Jagersfontein	Jagersfontein	Jagersfontein
Craton	Siberian craton	Siberian craton	Slave craton	Slave craton	Kaapvaal craton	Kaapvaal craton	Kaapvaal craton	Kaapvaal craton	Kaapvaal craton	Kaapvaal craton
Sample name	Km-88/23	Kr-119/13	Sl5-6	Sl5-86	JF-01	JF-09	JF-22	JF-37	JF-39	JF-42
(b) Eclogitic										
SiO_2	41.3	40.8	42.1	40.1	42.6	42.4	48.7	42.4	45.2	43.4
TiO_2	1.9	0.41	0.44	1.44	0.14	0.09	0.5	0.18	0.31	0.54
Al_2O_3	18	20.9	21.7	19.9	20	21	9.65	20.7	15	17.4
Cr_2O_3	0.05	0.07	0.07	0.02	0.24	0.08	0.22	0.13	0.24	0.03
FeO	16	14.1	15.5	20.2	12.6	14.1	11.7	12.9	10.8	12.9
MnO	0.29	0.31	0.34	0.36	0.42	0.4	0.36	0.38	0.24	0.36
MgO	8.82	9.41	16.6	7.19	17.6	16.2	21.7	16.9	20.3	13.4
CaO	12.2	12.9	3.03	10.6	6.14	6.11	5.73	6.43	5.67	11.16
Na_2O	0.93	0.43	0.33	0.38	0.15	0.2	0.65	0.14	0.37	0.54
Total	99.49	99.33	100.11	100.19	99.89	100.58	99.21	100.16	98.13	99.73
Si	3.13	3.07	3.06	3.06	3.10	3.08	3.55	3.08	3.32	3.22
Ti	0.11	0.02	0.02	0.08	0.01	0.00	0.03	0.01	0.02	0.03
Al	1.61	1.85	1.86	1.79	1.72	1.80	0.83	1.77	1.30	1.52
Cr	0.003	0.004	0.004	0.001	0.01	0.005	0.01	0.01	0.01	0.00
Fe	1.01	0.89	0.94	1.29	0.77	0.86	0.71	0.78	0.66	0.80
Mn	0.02	0.02	0.02	0.02	0.03	0.02	0.02	0.02	0.01	0.02
Mg	1.00	1.06	1.80	0.82	1.91	1.75	2.36	1.83	2.22	1.48
Ca	0.99	1.04	0.24	0.87	0.48	0.48	0.45	0.50	0.45	0.89
Na	0.14	0.06	0.05	0.06	0.02	0.03	0.09	0.02	0.05	0.08
Total	8.01	8.01	8.00	7.99	8.04	8.03	8.05	8.03	8.04	8.03
Pressure (GPa)[b]	12.9	11.8	8.0	10.9	9.3	9.1	15.0	9.1	12.0	13.0

Source	7	7	7	7	7
Mine	Jagersfontein	Jagersfontein	Jagersfontein	Jagersfontein	Jagersfontein
Craton	Kaapvaal craton	Kaapvaal craton	Kaapvaal craton	Kaapvaal craton	Kaapvaal craton
Sample name	JF-44	JF-48	JF-55	JF-58	JF-84
SiO_2	44.1	41.8	48	43.5	44.3
TiO_2	0.32	0.19	0.36	0.28	0.41
Al_2O_3	17.9	21.6	12.1	18.3	17.3
Cr_2O_3	0.31	0.11	0.36	0.18	0.3

Table 5 continued

Source	7	7	7	7	7
Mine	Jagersfontein	Jagersfontein	Jagersfontein	Jagersfontein	Jagersfontein
Craton	Kaapvaal craton	Kaapvaal craton	Kaapvaal craton	Kaapvaal craton	Kaapvaal craton
Sample name	JF-44	JF-48	JF-55	JF-58	JF-84
FeO	11.8	13.8	9.3	14.7	11.7
MnO	0.3	0.4	0.25	0.41	0.31
MgO	17.7	16.2	22	18.3	18.8
CaO	7.97	5.89	7.33	4.62	6.36
Na_2O	0.18	0.13	0.43	0.27	0.3
Total	100.58	100.12	100.13	100.56	99.78
Si	3.19	3.05	3.44	3.16	3.22
Ti	0.02	0.01	0.02	0.02	0.02
Al	1.53	1.86	1.02	1.57	1.48
Cr	0.02	0.01	0.02	0.01	0.02
Fe	0.71	0.84	0.56	0.89	0.71
Mn	0.02	0.02	0.02	0.03	0.02
Mg	1.91	1.76	2.35	1.98	2.03
Ca	0.62	0.46	0.56	0.36	0.49
Na	0.03	0.02	0.06	0.04	0.04
Total	8.03	8.02	8.05	8.05	8.03
Pressure (GPa)[b]	11.1	8.6	14.0	9.6	10.9

[a] Pressures calculated using Eq. 2

[b] Pressure calculated using Eq. 3

Source references [1] Moore and Gurney (1989), [2] Sobolev et al. (1997), [3] Hutchison (1997), [4] Sobolev et al. (2004), [5] Pokhilenko et al. (2004), [6] Banas et al. (2007), [7] Tappert et al. (2005), [8] Stachel and Harris (1997), [9] Moore and Gurney (1985), [10] Meyer and Mahin (1986)

peridotitic compositions, the sort that would be expected to form in normal "pyrolitic" mantle compositions, are also not very abundant (see Fig. 1). This suggest that these "unusual" depleted mantle lithologies, which are required for these high-Cr majoritic garnets to form, are actually rather common in the deep mantle, at least in the areas where diamonds grow and are subsequently transported to the surface by kimberlite volcanism.

Mineral densities in subducting slabs

We would like to add a short note on the effect of the garnet–pyroxene solid solution on the overall density of the mantle, as garnet is a lot denser than pyroxene (~3.8 and 3.4 at zero pressure, respectively, Irifune et al. 1986). If it is generally true that the majorite content in garnets in eclogitic is higher than for garnet in peridotitic compositions, this would contribute to the increased density of subducting slabs, which is what allows subducting slabs to sink into the mantle (Ganguly et al. 2009). However, van Mierlo et al. (2013) suggested that the diffusion rates of silicon into (majoritic) garnet are so slow, and that the majorite transformation in subducting slabs is inhibited unless the temperatures are very high. Furthermore, in depleted bulk compositions with high bulk Cr/(Cr + Al), the majorite content in garnet might be lower than in the surrounding fertile mantle which would increase the buoyancy of these regions. To explore this further, combined thermodynamic and geodynamic modeling is required.

Conclusions

We have performed experiments to determine the stability of the majorite component in garnet in a variety of bulk compositions, pressures, and temperatures. Our data show that the majorite content mainly depends on pressure, but also on garnet composition. The effect of temperature on the majorite substitution is negligible. We combined our data with the literature data and derived two empirical geobarometers, which can be used to estimate the pressure at which garnet equilibrated. Equation (2) is appropriate for majoritic garnet in peridotitic compositions, and Eq. (3) is recommended for majoritic garnets in eclogitic compositions. Our data show that majoritic garnets in an eclogitic composition will have a higher majorite content

compared to peridotitic majoritic garnets at the same pressure. Moreover, Cr-rich majoritic garnets have lower majorite content compared to Cr-poor garnets formed at the same pressure. This implies that Cr-rich majoritic garnet inclusions in diamonds must come from very deep in the asthenospheric mantle and must be derived from a high Cr, depleted mantle peridotite, e.g., a dunitic rock with very low garnet modes or a very high Cr/(Cr + Al) harzburgite.

Acknowledgments Our thanks go out to Jasper Berndt, Lukas Martin, Joachim Krause, and Beate Schmitte for their help with the microprobe measurements. Christof Kusebauch and Annette Wijbrans are thanked for their help with the fitting of the data. Christan Liebske and Natalia Stamm are thanked for their help with the multi-anvil experiments at the ETH. Furthermore, our thanks go to Michael Feldhaus, Heinz Heying, Jonas Kemmann, Andreas Boonk, Jürgen Schumacher, Ludger Buxtrup, and Andrew Hardes for their sterling efforts with the Münster multi-anvil apparatus. We would like to thank the editor Mark Ghiorso and two anonymous reviewers for their critical but constructive comments.

References

Akaogi M, Akimoto S (1977) Pyroxene-garnet solid-solution equilibria in systems $Mg_4Si_40_{12}$–$Mg_3Al_2Si_3O_{12}$ and $Fe_4Si_4O_{12}$–$Fe_3Al_2Si_3O_{12}$ at high-pressures and temperatures. Phys Earth Planet Inter 15(1):90–106

Akaogi M, Akimoto S (1979) High-pressure phase-equilibria in a garnet lherzolite, with special reference to Mg^{2+}–Fe^{2+} partitioning among constituent minerals. Phys Earth Planet Inter 19(1):31–51

Akaogi M, Navrotsky A, Yagii T, Akimoto S (1987) Pyroxene-garnet transformation: thermochemistry and elasticity of garnet solid solutions, and application to a pyrolite mantle. In: Manghnani MH, Syono Y (eds) High-pressure research in mineral physics. Terrapub, Tokyo, pp 251–260

Alifirova TA, Pokhilenko LN, Ovchinnikov YI, Donnelly CL, Riches AJV, Taylor LA (2012) Petrologic origin of exsolution textures in mantle minerals: evidence in pyroxenitic xenoliths from Yakutia kimberlites. Int Geol Rev 54(9):1071–1092

Banas A, Stachel T, Muehlenbachs K, McCandless TE (2007) Diamonds from the Buffalo Head Hills, Alberta: formation in a non-conventional setting. Lithos 93(1–2):199–213

Berry AJ, O'Neill HSC (2004) A XANES determination of the oxidation state of chromium in silicate glasses. Am Miner 89(5–6):790–798

Bindi L, Dymshits AM, Bobrov AV, Litasov KD, Shatskiy AF, Ohtani E, Litvin YA (2011) Crystal chemistry of sodium in the Earth's interior: the structure of $Na_2MgSi_5O_{12}$ synthesized at 17.5 GPa and 1700 degrees C. Am Miner 96(2–3):447–450

Bobrov AV, Kojitani H, Akaogi M, Litvin YA (2008) Phase relations on the diopside-jadeite-hedenbergite join up to 24 GPa and stability of Na-bearing majoritic garnet. Geochim Cosmochim Acta 72(9):2392–2408

Bose K, Ganguly J (1995) Quartz-coesite transition revisited—reversed experimental-determination at 500-1200-degrees-C and retrieved thermochemical properties. Am Miner 80(3–4):231–238

Boyd FR (1989) Compositional distinction between oceanic and cratonic lithosphere. Earth Planet Sci Lett 96(1–2):15–26

Boyd FR, Gurney JJ, Richardson SH (1985) Evidence for a 150–200-km thick archean lithosphere from diamond inclusion thermobarometry. Nature 315(6018):387–389

Brey GP, Bulatov VK, Girnis AV (2008) Geobarometry for peridotites: experiments in simple and natural systems from 6 to 10 GPa. J Petrol 49(1):3–24

Collerson KD, Hapugoda S, Kamber BS, Williams Q (2000) Rocks from the mantle transition zone: majorite-bearing xenoliths from malaita, southwest pacific. Science 288(5469):1215–1223

Collerson KD, Williams Q, Kamber BS, Omori S, Arai H, Ohtani E (2010) Majoritic garnet: a new approach to pressure estimation of shock events in meteorites and the encapsulation of sublithospheric inclusions in diamond. Geochim Cosmochim Ac 74(20):5939–5957

Cookenboo HO, Grutter HS (2010) Mantle-derived indicator mineral compositions as applied to diamond exploration. Geochem: Explor Environ, Anal 10(1):81–95

Davies RA, Griffin WL, O'Reilly SY, McCandless TE (2004) Inclusions in diamonds from the K14 and K10 kimberlites, Buffalo Hills, Alberta, Canada: diamond growth in a plume? Lithos 77(1–4):99–111

Degtyareva O, McMahon MI, Nelmes RJ (2004) High-pressure structural studies of group-15 elements. High Pressure Res 24:319–356

Doroshev AM, Brey GP, Girnis AV, Turkin AI, Kogarko LN (1997) Pyrope-knorringite garnets in the earths mantle: experiments in the MgO–Al_2O_3–SiO_2–Cr_2O_3 system. Geol Geofiz 38(2):523–545

Draper DS, Xirouchakis D, Agee CB (2003a) Trace element partitioning between garnet and chondritic melt from 5 to 9 GPa: implications for the onset of the majorite transition in the martian mantle. High Press Res 24(3):319–356

Draper DS, Xirouchakis D, Agee CB (2003b) Trace element partitioning between garnet and chondritic melt from 5 to 9 GPa: implications for the onset of the majorite transition in the martian mantle. Phys Earth Planet Inter 139(1–2):149–169

Dymshits AM, Bobrov AV, Bindi L, Litvin YA, Litasov KD, Shatskiy AF, Ohtani E (2013) Na-bearing majoritic garnet in the $Na_2MgSi_5O_{12}$–$Mg_3Al_2Si_3O_{12}$ join at 11–20 GPa: phase relations, structural peculiarities and solid solutions. Geochim Cosmochim Acta 105:1–13

Dymshits AM, Litasov KD, Sharygin IS, Shatskiy A, Ohtani E, Suzuki A, Funakoshi K (2014) Thermal equation of state of majoritic knorringite and its significance for continental upper mantle. J Geophys Res Solid Earth 119(11):8034–8046

Frost DJ (2003) The structure and sharpness of (Mg, Fe)(2)SiO4 phase transformations in the transition zone. Earth Planet Sci Lett 216(3):313–328

Frost DJ (2008) The upper mantle and transition zone. Elements 4(3):171–176

Ganguly J, Freed AM, Saxena SK (2009) Density profiles of oceanic slabs and surrounding mantle: integrated thermodynamic and thermal modeling, and implications for the fate of slabs at the 660 km discontinuity. Phys Earth Planet Inter 172(3–4):257–267

Gasparik T (1989) Transformation of enstatite–diopside–jadeite pyroxenes to garnet. Contrib Miner Petrol 102(4):389–405

Gasparik T (2002) Experimental investigation of the origin of majoritic garnet inclusions in diamonds. Phys Chem Miner 29(3):170–180

Girnis AV, Brey GP, Doroshev AM, Turkin AI, Simon N (2003) The system MgO–Al_2O_3–SiO_2–Cr_2O_3 revisited: reanalysis of Doroshev et al.'s (1997) experiments and new experiments. Eur J Mineral 15(6):953–964

Green DH, Falloon TJ (1998) Pyrolite: a Ringwood concept and its current expression. In: Jackson INS (ed) The Earth's mantle; composition, structure, and evolution. Cambridge University Press, Cambridge, pp 311–378

Grutter HS, Gurney JJ, Menzies AH, Winter F (2004) An updated classification scheme for mantle-derived garnet, for use by diamond explorers. Lithos 77(1–4):841–857

Gurney JJ, Switzer GS (1973) Discovery of garnets closely related to diamonds in Finsch Pipe, South-Africa. Contrib Mineral Petrol 39(2):103–116

Haggerty SE, Sautter V (1990) Ultradeep (Greater Than 300 Kilometers), Ultramafic Upper Mantle Xenoliths. Science 248(4958):993–996

Harte B (2010) Diamond formation in the deep mantle: the record of mineral inclusions and their distribution in relation to mantle dehydration zones. Miner Mag 74(2):189–215

Herzberg C, Zhang JZ (1996) Melting experiments on anhydrous peridotite KLB-1: compositions of magmas in the upper mantle and transition zone. J Geophys Res Solid Earth 101:8271–8295

Hirose K (2002) Phase transitions in pyrolitic mantle around 670-km depth: implications for upwelling of plumes fromthe lower mantle. J Geophys Res Solid Earth 107. doi:10.1029/2001JB000597

Hutchison MT (1997) Constitution of the deep transition zone and lower mantle shown by diamonds and their inclusions. PhD Thesis, University of Edinburgh

Irifune T (1987) An experimental investigation of the pyroxene garnet transformation in a pyrolite composition and its bearing on the constitution of the mantle. Phys Earth Planet Inter 45(4):324–336

Irifune T, Ohtani E, Kumazawa M (1982) Stability field of knorringite $Mg_3Cr_2Si_3O_{12}$ at high-pressure and its implication to the occurrence of Cr-rich pyrope in the upper mantle. Phys Earth Planet Inter 27(4):263–272

Irifune T, Sekine T, Ringwood AE, Hibberson WO (1986) The eclogite–garnetite transformation at high-pressure and some geophysical implications. Earth Planet Sci Lett 77(2):245–256

Jacob DE (2004) Nature and origin of eclogite xenoliths from kimberlites. Lithos 77(1–4):295–316

Kaminsky FV, Zakharchenko OD, Davies R, Griffin WL, Khachatryan-Blinova GK, Shiryaev AA (2001) Superdeep diamonds from the Juina area, Mato Grosso State, Brazil. Contrib Mineral Petrol 140(6):734–753

Kato T (1986) Stability relation of (Mg, Fe)SiO3 garnets, major constituents in the earths interior. Earth Planet Sci Lett 77(3–4):399–408

Kawamoto T (2004) Hydrous phase stability and partial melt chemistry in H(2)O-saturated KLB-1 peridotite up to the uppermost lower mantle conditions. Phys Earth Planet Inter 143:387–395

Kesson SE, Ringwood AE, Hibberson WO (1994) Kimberlite melting relations revisited. Earth Planet Sci Lett 121:261–262

Kiseeva ES, Litasov KD, Yaxley GM, Ohtani E, Kamenetsky VS (2013a) Melting and phase relations of carbonated eclogite at 9–21 GPa and the petrogenesis of alkali-rich melts in the deep mantle. J Petrol 54(8):1555–1583

Kiseeva ES, Yaxley GM, Stepanov AS, Tkalcic H, Litasov KD, Kamenetsky VS (2013b) Metapyroxenite in the mantle transition zone revealed from majorite inclusions in diamonds. Geology 41(8):883–886

Klemme S (2004) The influence of Cr on the garnet-spinel transition in the Earth's mantle: experiments in the system MgO–Cr_2O_3–SiO_2 and thermodynamic modelling. Lithos 77(1–4):639–646

Klemme S, O'Neill HSC (1997) The reaction $MgCr_2O_4 + SiO_2 = Cr_2O_3 + MgSiO_3$ and the free energy of formation of magnesiochromite ($MgCr_2O_4$). Contrib Miner Petrol 130(1):59–65

Klemme S, O'Neill HSC (2000a) The near-solidus transition from garnet lherzolite to spinel lherzolite. Contrib Miner Petrol 138(3):237–248

Klemme S, O'Neill HSC (2000b) The effect of Cr on the solubility of Al in orthopyroxene: experiments and thermodynamic modelling. Contrib Miner Petrol 140(1):84–98

Li JP, O'Neill HSC, Seifert F (1995) Subsolidus phase-relations in the system MgO–SiO_2–Cr–O in equilibrium with metallic Cr, and their significance for the petrochemistry of chromium. J Petrol 36(1):107–132

Litasov KD, Ohtani E (2005) Phase relations in hydrous MORB at 18–28 GPa: implications for heterogeneity of the lower mantle. Phys Earth Planet Inter 150(4):239–263

Meyer HOA, Mahin RA (1986) The kimberlites of Guinea, West Africa. Geological Society of Australia, Abstract Series, In Proceedings of 4th international kimberlite conference, vol 16, pp 66–76

Moore RO, Gurney JJ (1985) Pyroxene solid-solution in garnets included in diamond. Nature 318(6046):553–555

Moore RO, Gurney JJ (1989) Mineral inclusions in diamond from the Monastery kimberlite, South Africa. In Kimberlites and related rocks, Vol 2 (ed. J. Ross et al.), pp. 1029–1041. Proceedings of 4th international kimberlite conference, Perth, 1986. Geol. Soc. Australia Spec. Publ. 14

Nishihara Y, Takahashi E (2001) Phase relation and physical properties of an Al-depleted komatiite to 23 GPa. Earth Planet Sci Lett 190(1–2):65–77

O'Neill HSC (1981) The transition between spinel lherzolite and garnet lherzolite, and its use as a geobarometer. Contrib Miner Petrol 77(2):185–194

Ohtani E, Kawabe I, Moriyama J, Nagata Y (1989) Partitioning of elements between majorite garnet and melt and implications for petrogenesis of komatiite. Contrib Miner Petr 103:263–269

Okamoto K, Maruyama S (2004) The eclogite-gametite transformation in the MORB + H_2O system. Phys Earth Planet Inter 146(1–2):283–296

Ono S, Yasuda A (1996) Compositional change of majoritic garnet in a MORB composition from 7 to 17 GPa and 1400 to 1600 degrees C. Phys Earth Planet Inter 96(2–3):171–179

Ono S, Ito E, Katsura T (2001) Mineralogy of subducted basaltic crust (MORB) from 25 to 37 GPa, and chemical heterogeneity of the lower mantle. Earth Planet Sci Lett 190(1–2):57–63

Pokhilenko NP, Sobolev NV, Reutsky VN, Hall AE, Taylor LA (2004) Crystalline inclusions and C isotope ratios in diamonds from the Snap Lake/King Lake kimberlite dyke system: evidence of ultradeep and enriched lithospheric mantle. Lithos 77(1–4):57–67

Ringwood AE (1967) Pyroxene-garnet transformation in earths mantle. Earth Planet Sci Lett 2(3):255–263

Ringwood AE (1977) Synthesis of pyrope-knorringite solid-solution series. Earth Planet Sci Lett 36(3):443–448

Ringwood AE, Major A (1966) High-pressure transformations in pyroxenes. Earth Planet Sci Lett 1(5):351–357

Ringwood AE, Major A (1971) Synthesis of majorite and other high-pressure garnets and perovskites. Earth Planet Sci Lett 12(4):411–418

Roden MF, Patino-Douce AE, Jagoutz E, Laz'ko EE (2006) High pressure petrogenesis of Mg-rich garnet pyroxenites from Mir kimberlite, Russia. Lithos 90(1–2):77–91

Rohrbach A, Schmidt MW (2011) Redox freezing and melting in the earth's deep mantle resulting from carbon-iron redox coupling. Nature 472(7342):209–212

Rohrbach A, Ballhaus C, Golla-Schindler U, Ulmer P, Kamenetsky VS, Kuzmin DV (2007) Metal saturation in the upper mantle. Nature 449(7161):456–458

Rohrbach A, Ballhaus C, Ulmer P, Golla-Schindler U, Schonbohm D (2011) Experimental evidence for a reduced metal-saturated upper mantle. J Petrol 52(4):717–731

Sautter V, Haggerty SE, Field S (1991) Ultradeep (greater-than-300 kilometers) ultramafic xenoliths—petrological evidence from the transition zone. Science 252(5007):827–830

Scambelluri M, Pettke T, van Roermund HLM (2008) Majoritic garnets monitor deep subduction fluid flow and mantle dynamics. Geology 36(1):59–62

Schulze DJ (2003) A classification scheme for mantle-derived garnets in kimberlite: a tool for investigating the mantle and exploring for diamonds. Lithos 71(2–4):195–213

Sirotkina EA, Bobrov AV, Bindi L, Irifune T (2015) Phase relations and formation of chromium-rich phases in the system $Mg_4Si_4O_{12}$–$Mg_3Cr_2Si_3O_{12}$ at 10–24 GPa and 1600 degrees C. Contrib Mineral Petrol 169(1)

Sobolev NV, Lavrente YG, Pokhilen NP, Usova LV (1973) Chrome-rich garnets from kimberlites of Yakutia and their parageneses. Contrib Mineral Petrol 40(1):39–52

Sobolev NV, Yefimova ES, Reimers LF, Zakharchenko OD, Makhin AI, Usova LV (1997) Mineral inclusions in diamonds from the Arkhangelsk kimberlite province. Geol Geofiz 38(2):358–370

Sobolev NV, Logvinova AM, Zedgenizov DA, Seryotkin YV, Yefimova ES, Floss C, Taylor LA (2004) Mineral inclusions in microdiamonds and macrodiamonds from kimberlites of Yakutia: a comparative study. Lithos 77(1–4):225–242

Stachel T (2001) Diamonds from the asthenosphere and the transition zone. Eur J Miner 13(5):883–892

Stachel T, Harris JW (1997) Diamond precipitation and mantle metasomatism—evidence from the trace element chemistry of silicate inclusions in diamonds from Akwatia, Ghana. Contrib Miner Petrol 129(2–3):143–154

Stachel T, Harris JW (2008) The origin of cratonic diamonds—constraints from mineral inclusions. Ore Geol Rev 34(1–2):5–32

Stewart AJ, van Westrenen W, Schmidt MW, Melekhova E (2006) Effect of gasketing and assembly design: a novel 10/3.5 mm multi-anvil assembly reaching perovskite pressures. High Press Res 26:293–299

Susaki J, Akaogi M, Akimoto S, Shimomura O (1985) Garnet-perovskite transformation in $CaGeO_3$—in situ X-Ray measurements using synchrotron radiation. Geophys Res Lett 12(10):729–732

Tappert R, Stachel T, Harris JW, Muehlenbachs K, Ludwig T, Brey GP (2005) Diamonds from Jagersfontein (South Africa): messengers from the sublithospheric mantle. Contrib Miner Petrol 150(5):505–522

Thomson AR, Walter MJ, Kohn SC, Brooker RA (2016) Slab melting as a barrier to deep carbon subduction. Science 529(7584):76–79

Ulmer P, Sweeney RJ (2002) Generation and differentiation of group II kimberlites: constraints from a high-pressure experimental study to 10 GPa. Geochim Cosmochim Acta 66:2139–2153

van der Hilst RD, Widiyantoro S, Engdahl ER (1997) Evidence for deep mantle circulation from global tomography. Nature 386(6625):578–584

van Mierlo WL, Langenhorst F, Frost DJ, Rubie DC (2013) Stagnation of subducting slabs in the transition zone due to slow diffusion in majoritic garnet. Nat Geosci 6(5):400–403

van Roermund HLM, Drury MR, Barnhoorn A, De Ronde AA (2000) Super-silicic garnet microstructures from an orogenic garnet peridotite, evidence for an ultra-deep (> 6 GPa) origin. J Metamorph Geol 18(2):135–147

van Roermund HLM, Drury MR, Barnhoorn A, De Ronde A (2001) Relict majoritic garnet microstructures from ultra-deep orogenic peridotites in western Norway. J Petrol 42(1):117–130

Walter MJ (1998) Melting of garnet peridotite and the origin of komatiite and depleted lithosphere. J Petrol 39(1):29–60

Walter MJ (2003) Melt extraction and compositional variability in mantle lithosphere. In: Carlson RW, Holland HD, Turekian KK (eds) Treatise on geochemistry: the mantle and core, vol 2. Elsevier, Amsterdam, pp 363–394

Walter MJ, Kohn SC, Araujo D, Bulanova GP, Smith CB, Gaillou E, Wang J, Steele A, Shirey SB (2011) Deep mantle cycling of oceanic crust: evidence from diamonds and their mineral inclusions. Science 333(6052):54–57

Wang WY, Takahashi E (2000) Subsolidus and melting experiments of K-doped peridotite KLB-1 to 27 GPa: its geophysical and geochemical implications. J Geophys Res Solid Earth 105(B2):2855–2868

Widiyantoro S, van der Hilst R (1996) Structure and evolution of lithospheric slab beneath the Sunda arc, Indonesia. Science 271(5255):1566–1570

Wijbrans CH, Niehaus O, Rohrbach A, Pottgen R, Klemme S (2014) Thermodynamic and magnetic properties of knorringite garnet ($Mg_3Cr_2Si_3O_{12}$) based on low-temperature calorimetry and magnetic susceptibility measurements. Phys Chem Miner 41(5):341–346

Wood BJ, Kiseeva ES, Matzen AK (2013) Garnet in the earth's mantle. Elements 9(6):421–426

Yang JS, Dobrzhinetskaya L, Bai WJ, Fang QS, Rolbinson PT, Zhang J, Green HW (2007) Diamond- and coesite-bearing chromitites from the Luobusa ophiolite, Tibet. Geology 35(10):875–878

Yang JS, Robinson PT, Dilek Y (2014) Diamonds in ophiolites. Elements 10(2):127–130

Yasuda A, Fujii T, Kurita K (1994) Melting phase-relations of an anhydrous midocean ridge basalt from 3 to 20 GPa—implications for the behavior of subducted oceanic-crust in the mantle. J Geophys Res Solid Earth 99(B5):9401–9414

Zhang J, Li B, Utsumi W, Liebermann RC (1996) In situ X-ray observations of the coesite stishovite transition: reversed phase boundary and kinetics. Phys Chem Miner 23(1):1–10

Zhang RY, Zhai SM, Fei YW, Liou JG (2003) Titanium solubility in coexisting garnet and clinopyroxene at very high pressure: the significance of exsolved rutile in garnet. Earth Planet Sci Lett 216(4):591–601

Zou YT, Irifune T (2012) Phase relations in $Mg_3Cr_2Si_3O_{12}$ and formation of majoritic knorringite garnet at high pressure and high temperature. J Miner Petrol Sci 107(5):197–205